Naval Research Laboratory

Washington, DC 20375-5320

NRL/MR/6750--11-9333

Experimental and Theoretical Estimation of Excited Species Generation in Pulsed Electron Beam–Generated Plasmas Produced in Pure Argon, Nitrogen, Oxygen, and Their Mixtures

E.H. LOCK
R.F. FERNSLER

Charged Particle Physics Branch
Plasma Physics Division

S. SLINKER

Beam Physics Branch
Plasma Physics Division

S.G. WALTON

Charged Particle Physics Branch
Plasma Physics Division

May 13, 2011

REPORT DOCUMENTATION PAGE

Form Approved
OMB No. 0704-0188

1. REPORT DATE *(DD-MM-YYYY)*	**2. REPORT TYPE**	**3. DATES COVERED** *(From - To)*
13-05-2011	Memorandum Report	

4. TITLE AND SUBTITLE

Experimental and Theoretical Estimation of Excited Species Generation in Pulsed Electron Beam–Generated Plasmas Produced in Pure Argon, Nitrogen, Oxygen, and Their Mixtures

5a. CONTRACT NUMBER

5b. GRANT NUMBER

5c. PROGRAM ELEMENT NUMBER

6. AUTHOR(S)

E.H. Lock, R.F. Fernsler, S. Slinker, and S.G. Walton

5d. PROJECT NUMBER

67-9870-01

5e. TASK NUMBER

5f. WORK UNIT NUMBER

7. PERFORMING ORGANIZATION NAME(S) AND ADDRESS(ES)

Naval Research Laboratory
4555 Overlook Avenue, SW
Washington, DC 20375-5320

8. PERFORMING ORGANIZATION REPORT NUMBER

NRL/MR/6750--11-9333

9. SPONSORING / MONITORING AGENCY NAME(S) AND ADDRESS(ES)

Office of Naval Research
One Liberty Center
875 North Randolph Street, Suite 1425
Arlington, VA 22203-1995

10. SPONSOR / MONITOR'S ACRONYM(S)

ONR

11. SPONSOR / MONITOR'S REPORT NUMBER(S)

12. DISTRIBUTION / AVAILABILITY STATEMENT

Approved for public release; distribution is unlimited.

13. SUPPLEMENTARY NOTES

14. ABSTRACT

In this report we use optical emission spectroscopy (OES) to determine the excited species produced by a high energy pulsed electron beam (2 kV) in various gases. The gases studied include pure argon, nitrogen, oxygen, and argon/nitrogen and argon/oxygen mixtures. The application of OES as an electron beam diagnostic method is evaluated. The experimental results are compared with theoretical predictions.

15. SUBJECT TERMS

Optical emission spectroscopy Excited species
Plasma

16. SECURITY CLASSIFICATION OF:			**17. LIMITATION OF ABSTRACT**	**18. NUMBER OF PAGES**	**19a. NAME OF RESPONSIBLE PERSON**
a. REPORT	**b. ABSTRACT**	**c. THIS PAGE**			Evgeniya Lock
Unclassified	Unclassified	Unclassified	UL	63	**19b. TELEPHONE NUMBER** *(include area code)* (202) 767-0351

Standard Form 298 (Rev. 8-98)
Prescribed by ANSI Std. Z39.18

Table of Contents

1. Introduction

Non-destructive diagnostics methods have been extensively developed for relativistic or mildly relativistic electron beams to determine the electron beam transient and thus the pulse shape and width[1], the beam temporal and spatial velocity, and current (energy) distributions[2-4]. The beams that are of interest in this work are produced by 2 keV electrons and have been extensively used for material processing applications like thin film deposition, etching, nitriding, polymer metallization and more recently polymer and graphene functionalization [5-7]. However, in order to understand the observed material modifications precise characterization of the beam current density and energy depositions, plasma densities and electron temperatures are needed. In previous studies, Langmuir and frequency probes, and mass spectroscopy [8-11] were applied to characterize the electron temperature and plasma density, ion flux and ion energy respectively. However, application of probes pertubate the beam and thus non-destructive diagnostics methods represent an attractive alternative. Furthermore, the generation of excited species in electron beam-generated plasmas had not been investigated and thus guided by the earlier theoretical analyses, the goals of this work are: (1) to identify the excited species in argon, oxygen, nitrogen and Ar/O_2 and Ar/N_2 mixtures using optical emission spectroscopy (OES), and (2) to evaluate the suitability of OES as a diagnostic for determining both the spatial profile of electron beams and variations in neutral gas density.

Optical emission spectroscopy is based on analyzing the light emitted by neutral or ionized atoms, radicals, or molecules which have been electronically excited by collisions with energetic electrons, and the technique is widely used as a diagnostic in plasma processing[12, 13]. OES can be used for excited species characterization, photon flux determination as a function of wavelength, for actinometry, and as a diagnostic for electron beams. Advantages of using optical emission spectroscopy include (i) OES is non-intrusive; (ii) A large excitation cross section produces a strong signal; (iii) Emission from optically allowed states is insensitive to beam energy. (iv) A short lifetime makes for good temporal response and fewer complications from quenching. (v) A large excitation energy minimizes the excitation caused both by "plasma" electrons and radiative cascade. (vi) Data interpretation is direct and easy when quenching and photon re-absorption (within the medium and outside) are weak; both effects can be included if necessary, however.

It should be noted that the emission spectrum obtained in electron beam-generated plasmas is largely independent of electron temperature and thus cannot be used for its determination. Furthermore, while much theoretical work has been done in this area[14-19] with some discussion of experimental results,[20, 21]. Detailed comparisons between theory and experiments are generally lacking. By contrast, application of OES to conventional discharges in pure argon, oxygen and nitrogen and their mixtures is well established.[22-26]

Manuscript approved April 12, 2011.

2. Optical emission spectroscopy fundamentals

Interpreting the emission spectrum requires identifying the routes to excitation. The emission is detected as bands, lines and continuum emissions [27].The band emission results from the decay of excited molecular ions or neutrals into different rotational and vibrational levels, and the processes that lead to band emission are

(1) Direct excitation and ionization (e.g. First Negative Band of N_2^+)
$e + A_2 \rightarrow (A_2^+)^* + e$
(2) Direct excitation (e.g. First and Second Positive Band of N_2)
$e + A_2 \rightarrow A_2^* + e$
(3) Vibrational excitation (e.g. nitrogen)
$e + A_2 \rightarrow A_2'' + e$
(4) Chemiluminescence (infrared NO emissions)
$B^* + A_2 \rightarrow AB'' + A$

Here A_2 is a molecule, A is an atom, A_2^* is an electronically molecule, A_2'' is a vibrationally excited molecule, $(A_2^+)^*$ is an excited molecular ion, B* is an excited atom, and AB'' is a vibrationally excited molecule.

Line emission occurs through the decay of excited atoms and atomic ions. These excited states are produced by

(1) Direct excitation
$e + A \rightarrow A^* + e$
$e + A^+ \rightarrow (A^+)^* + e$
(2) Dissociative excitation
$e + A_2 \rightarrow A^* + A + e$
(3) Dissociative ionization with excitation
$e + A_2 \rightarrow A^* + A^+ + 2e$
$e + A_2 \rightarrow A + (A^+)^* + 2e$
(4) Dissociative recombination of molecular ion with charged species
$e + AB^+ \rightarrow A + B^*$
(5) Radiative and collisional recombination
$e + A^+ \rightarrow A^* + h\nu$

3. Theoretical model

In this report the particle-in-cell simulation PLUME code[8] was used. PLUME follows the beam electrons and the daughter electrons created by ionization in both space and time, until their energy falls below a cutoff, nominally 10 eV. Only binary collisions between electrons and ground-state neutrals are treated, and therefore processes like electron-electron collisions are ignored. This approach is well justified provided the degree of gas ionization and excitation is very low. Given this model, the following conditions hold:

1. Gas excitation rates are determined by the beam current I_b and beam energy E_b, with little or no dependence on the plasma electron density n_e or temperature T_e.
2. The ratio of any two rates is largely independent of I_b, E_b, n_e and T_e provided
    a. The initial beam energy exceeds 1 keV

b. The excitation energies satisfy $W_i > 5T_e$

Below 1 keV the structure of the cross sections becomes more complicated, while below $5T_e$ the contribution from the plasma electrons can no longer be ignored.

a) ***Volumetric light emission intensity***

The volumetric intensity at which excited species *i* emits light is given by

$$P_i = h\nu_i \frac{dn_i}{dt},$$

where $h\nu_i$ is the photon energy and dn_i/dt is the production rate of every state. The emission reaches the value given by the formula within a few radiative lifetimes τ_i after the start of the beam. It should be noted that this formula accounts only for direct excitation of state *i* by the beam. PLUME does not follow excited species after they are created. However, for light emitted from a state *i* with frequency ν_k having more than one decay path, the volumetric intensity is given by

$$P_k = \left(\frac{\tau_{ki}^{-1}}{\sum_q \tau_{qi}^{-1}} \right) \frac{h\nu_k dn_i}{dt},$$

where the sum over q includes all possible decay paths. However, regardless of the source, each state *i* is produced from gas constituent *j* at a volumetric rate given by

$$\frac{dn_i}{dt} = \frac{1}{\varepsilon_i} \frac{dE_j}{dt},$$

where dE_j/dt is the volumetric rate at which gas constituent j absorbs energy at a given point in space and ε_i is the mean energy per state. Thus, knowing that for a given gas the energy of the emitted photons is almost constant, the most important factor that influences production rate of each state and the light emission intensity is the mean energy per state ε_i - the production efficiency varies inversely with ε_i for each state. The latter is discussed in the following section in more detail because its proper understanding is critical for the following data interpretation and comparison between theory and experiment.

b) ***Mean energy per state***

As mentioned above, the excitation, ionization and gas dissociation processes can be characterized in terms of the mean energy ε_i needed to create a given state. The mean energies are nearly constant for high energy beams[28] (> 1 kV) but not for discharges. For example, the electron energy ε_0 needed to create an electron–ion pair is 36 eV in nitrogen and 28 eV in oxygen. These values are slightly more than twice the ground state ionization energies, and thus approximately half of the beam energy is spent on ionization. Moreover, the mean energy is approximately 30 eV in all gases, independent of beam current and energy.

The fact that the mean energies ε_i are nearly constant for high energy beams is well known but rarely explained. The underlying reason can be found in the Born-Bethe collision model, which applies when incident electrons have kinetic energies exceeding $30W_{iz} \sim 500$ eV, where W_{iz} is the ionization energy of the target molecules. Electrons (v_{pe}) satisfying this conditions have much higher velocities then the bound atom electrons (v_{ae}) ($v_{pe} >> v_{ae}$), so the bound electrons can be treated as free and at rest. At this condition, the energy transferred to the bound electron is depends on the primary electrons characteristics, i.e. their charge (*ze*) and velocity (*v*), the number of atoms per unit volume (*N*) (gas density) but most importantly on the number of bound electrons (Z) per atom as shown in the formula below:

$$\frac{dE}{dx} = 4\pi NZ\frac{z^2e^4}{mv^2}lnB$$

where B is a ratio of the maximum to minimum impact factors and because B is in the logarithm it is of negligible importance[29]. Thus, the number of the bound valence electrons rather than the atom structure determines the total energy loss. The importance of valence electrons on the total electron energy loss is also discussed by Fridman and Kennedy[30]. However, how the energy is lost, i.e. how the energy is distributed among the specific ionization and excitation channels will be determined by the *specific* atomic gas structure. Most of the electron energy of the primary electrons goes primary into creating ions and thus high-energy secondary electron population, i.e. high-energy tail of the electron energy distribution f(ε), is produced. It should be noted that part of the electron energy is spend on gas dissociation and excitation and most of the optically allowed excited states are produced by the high energy electrons as well.

The unnormalized electron energy distribution from PLUME (averaged over all space) obtained when electron beam passes through a different media (nitrogen, oxygen, argon and two gas mixtures) is shown in Figure 1. The distributions are similar down to 20 eV, with minor differences in pure oxygen and pure argon. Oxygen lacks electronic states between 6.1 and 12.1 eV, while the model used for Ar excludes all ion states above 15.76 eV. The lack of electronic states below 11.55 eV in argon explains the sharp rise in f(ε) seen below 20 eV. The sudden fall at 11.6 eV occurs because PLUME does not follow electrons below that energy. However, in all cases the population of low energy electrons $\varepsilon < 10$ eV, $f(\varepsilon) = 10^7$ is the highest. These electrons, with energies lower than the ionization potential (W_i) are called plasma electrons. They are the ones that determine the plasma properties – electron temperature, plasma potential and plasma density. The electrons with energies higher than the W_i that can further ionize and excite the gas are termed secondary electrons. Their population is several orders of magnitude lower than the plasma electrons.

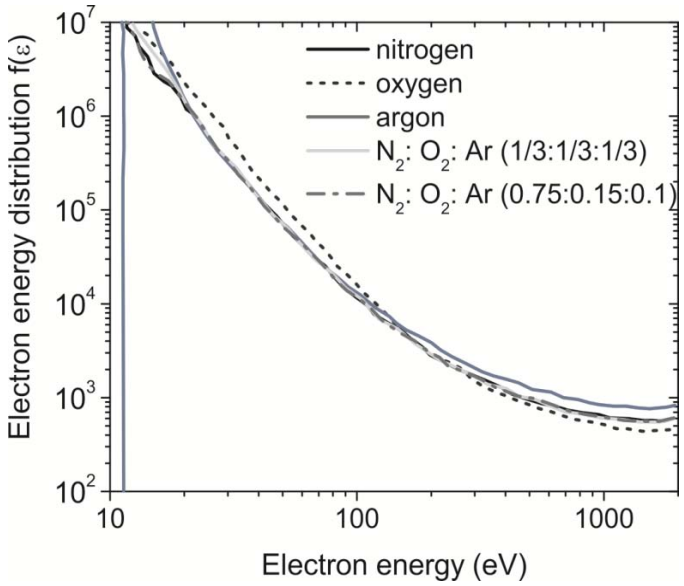

Figure 1. Electron energy distribution function for pure nitrogen, oxygen, argon and $N_2/O_2/Ar$ mixtures with two mixture concentrations: 75 %, 15 %, 10 % and 33.3 %, 33.3 %, 33.3 %. The initial beam energy is 2 kV.

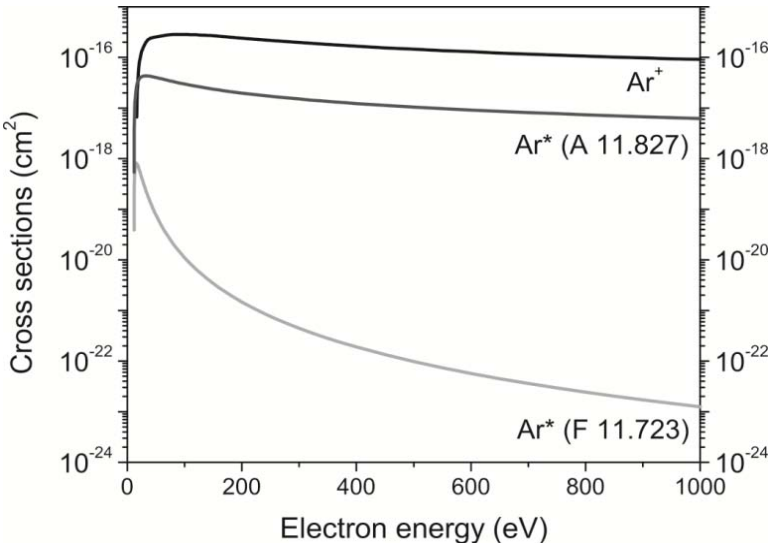

Figure 2. Ionization and excitation cross sections in argon. A denoted allowed excited state and F denotes forbidden excited state.

c) ***Cross sections***

Cross section is a fundamental quantity that characterizes each collisional process between high energy electron and a "target" gas particle. Detailed studies of electron energy deposition in specific gases requires a complete set of cross sections for electron impact excitation and ionization of constituent species over a wide energy range of the incident electrons. Ionization and excitation cross sections of allowed and forbidden states in argon are shown in Figure 2. It is obvious that the cross sections are a strong function of electron energy. The cross sections for optically allowed states and ionization fall off similarly with energy above a few hundred eV, so the fraction of energy going into each of these states is nearly constant, as is ε_i. The cross sections for optically forbidden states fall off faster with energy, so the mean energy per state is more sensitive to the low energy portion of electron energy distribution f(ε). And because the atomic structure strongly affects f(ε) at low energy, ε_i depends more strongly on gas composition. The dependence is the strongest for states having the fastest falloff in energy, and for those states ε_i can be treated as constant only if the gas composition is fixed and $W_i > 5T_e$.

Excellent collections of cross sections for electron collisions with N_2, O_2, O, N, O^+, N^+ have been compiled by A. W. Ali[31] and R. D. Taylor[32]. It should be noted that usually excitation cross sections are measured at low energies and finding a proper way to extend a cross section to high energies e.g. 1 keV is not trivial. There are a number of formulas used for extension of ionization cross sections to high energies, but Bethe formula[32] is the most commonly applied ($\sigma \sim \ln E/E$). For optically allowed and forbidden states of oxygen atoms Drawin's formulas have been applied and the coefficients needed for the cross sections estimations have been published by Slinker[14]. However, as noted by A. W. Ali[31] caution is needed for the cross section extension of every forbidden states. He has shown that for the excited states of nitrogen molecules the rate of cross section decay at high energies is different. Ali[31] suggests that for energies above 40 eV the cross sections of $A^3\Sigma$, $B^3\Pi$ states can be extended using the E^{-3} dependence, for the $C^3\Pi$ state the dependence is $E^{-2.2}$ and the singlet states $a'^1\Sigma$, $a'\Pi$, $w^1\Delta$ can be extended using the E^{-1} dependence. The reports also discuss the uncertainties in cross sections measurements.

An example of uncertainties in cross section estimation is shown in Figure 3 in the case of argon for two of the most important excited argon neutral states 2p9 (13.08 eV) and 2p1 (13.48 eV) responsible for the 811.5 nm and 750.4 nm emissions respectively. In PLUME Bretagne's cross sections were used and they are shown in the appendix. It should be noted that Bretagne et al.[17] modeled electrons beams in argon using an extensive set of inelastic cross sections,[16] but only results for certain states were published. As a comparison, the cross sections recommended by Hayashi,[33] Phelps,[34] and Boffard[35] are plotted as well. As is evident, the discrepancies in the cross sections for the 13.08 eV state are large, although in all cases, the cross sections for the 13.48 eV state are higher. The mean energies ε_i depend on the cross sections, and therefore uncertainties in the latter produce similar uncertainties in ε_i.

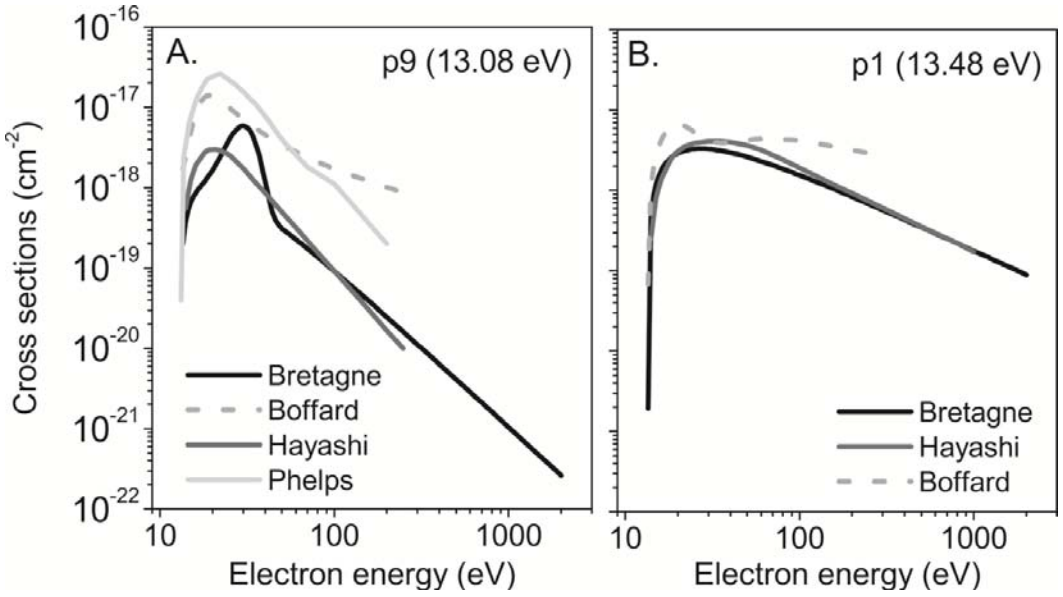

Figure 3. Comparison of cross sections for 13.08 eV and 13.48 eV states responsible for 811 nm and 750 nm lines respectively based on data by Bretagne, Hayashi, Phelps, and Boffard.

d) ***Theoretical results***

Results from two sets of simulations are reported here, at initial beam energies of 2 and 20 keV. However, since the values obtained for the mean energy per state ε_i differed by less than 5 %, only one value is given in the Tables I–IV, rounded off to 10 % for simplicity. The mean energy ε_0 per electron-ion pair equals the reciprocal of the sum over ε_i^{-1} for all types of ions, including some not shown in the tables.

i. Nitrogen and Oxygen

For the runs in nitrogen and oxygen the cutoff energy was lowered from 10 eV to 5 eV. The results for pure nitrogen are given in Table I, while those for pure oxygen summarized in Table 2. Unlike nitrogen, oxygen contains electronic states below 5 eV. Although PLUME computes ε_i for these states, the values are not listed because the actual values depend on n_e and T_e. That is, the plasma electrons contribute to the emission unless $T_e \leq 0.2$ eV. Included in the Tables I-IV are the excitation energy W_i (eV), the radiative lifetimes τ_i(s), the wavelengths λ_i(nm) of the emitted light, the mean energy per state ε_I (eV) and the production efficiency $\eta_i = W_i/\varepsilon_i$.

Table I. Theoretical results for nitrogen (ε_0 = 36 eV) for an initial beam energy of 2 keV

Transition	Lifetime τ_i (s)	Wavelength λ_i (nm)	Excitation energy W_i (eV)	Mean energy per state ε_i (eV)	Production efficiency η_i (-)
Nitrogen molecules (N_2)					
$A^3\Sigma \rightarrow X^1\Sigma_g$	13	293.0	6.17	210	0.029
$B^3\Pi \rightarrow A^3\Sigma$	7.5×10^{-6}	1045	7.35	230	0.032
$W^3\Delta \rightarrow X^1\Sigma_g$	6.5	208.0	7.36	310	0.024
$B'^3\Sigma \rightarrow B^3\Pi$	3×10^{-5}	1524	8.16	1100	0.007
$C^3\Pi \rightarrow B^3\Pi$	4.5×10^{-8}	337.1	11.0	620	0.018
$E^3\Sigma \rightarrow A^3\Sigma$	300	255.3	11.9	31,000	0.0004
$a'^1\Sigma \rightarrow A^3\Sigma$	0.7	177.1	8.39	1300	0.006
$a^1\Pi \rightarrow X^1\Sigma_g$	10^{-4}	155.2	8.55	430	0.019
$a^1\Pi \rightarrow a'^1\Sigma_g$	7.7×10^{-3}	8252			
$w^1\Delta \rightarrow a^1\Pi$	6.6×10^{-4}	3578	8.89	1200	0.007
$a''^1\Sigma$			12.2	3300	0.004
Nitrogen ions (N_2^+)					
$X^2\Sigma$			15.6	110	0.14
$A^2\Pi$			16.6	100	0.17
$B^2\Sigma \rightarrow X^2\Sigma$	6.6×10^{-8}	391.4	18.8	310	0.06

Table II. Theoretical results for oxygen (ε_0 = 28 eV) for an initial beam energy of 2 keV

Transition	Lifetime τ_i(s)	Wavelength λ_i (nm)	Excitation energy W_i (eV)	Mean energy per state ε_i (eV)	Production efficiency η_i (-)
Oxygen molecules (O_2)					
$a^1\Delta \rightarrow X^3\Sigma$	3.8×10^{3}	~1.27 mkm	0.98		
$b^1\Sigma \rightarrow X^3\Sigma$	12	~762	1.63		
$c^1\Sigma + A,^3\Delta + A^3\Sigma$	0.09	243-306	4.70		
$B^3\Sigma \rightarrow X^3\Sigma$	5×10^{-7}	~200	6.10	43	0.14
$B^3\Sigma \rightarrow O^* + O$	5×10^{-11}				
Oxygen ions (O_2^+)					
$X^3\Pi$			12.1	140	0.09
$a^4\Pi$			16.1	84	0.19
$A^2\Pi$			16.9	405	0.04
$b^4\Sigma \rightarrow a^4\Pi$	~ 10^{-6}	~ 600	18.2	240	0.08

Table III. Theoretical results for argon (ε_0 = 27 eV) for an initial beam energy of 2 keV

Transition	Lifetime τ_i(s)	Wavelength λ_i (nm)	Excitation energy W_i (eV)	Mean energy per state ε_i (eV)	Production efficiency η_i (-)
$4s(3/2)_2 \rightarrow 1S_0$	40	107.8	11.55	680*	0.017
$4s(3/2)_1 \rightarrow 1S_0$	8.4×10^{-9}	106.7	11.62	480	0.024
$4s'(1/2)_o \rightarrow 1S_0$	50	105.8	11.72	5600	0.002
$4s'(1/2)_1 \rightarrow 1S_0$	2×10^{-9}	104.8	11.83	140	0.085
$4p(1/2)_1 \rightarrow 4s\ (3/2)_{1,2}$	18, 5.3×10^{-8}	965.8, 912.3	12.91	6400	0.002
$4p(5/2)_3 \rightarrow 4s\ (3/2)_2$	3×10^{-8}	811.5	13.08	5400	0.002
$4p(5/2)_2 \rightarrow 4s\ (3/2)_{1,2}$	4.7, 11×10^{-8}	842.5, 801.5	13.09	5900	0.002
$4p(3/2)_1 \rightarrow 4s\ (3/2)_{1,2}$	40, 1.9×10^{-7}	810.4, 772.4	13.15	8200	0.002
$4p(3/2)_2 \rightarrow 4s\ (1/2)_{1,2}$	20, 4.1×10^{-8}	922.4, 763.5	13.17	6800	0.002
$4p(1/2)_0$+$4p'(3/2)_1$	7.1, 5.4, 2.5 x 10^{-8}	852.1, 794.8, 751.5	13.28	4200	0.003
$4p'(3/2)_2 \rightarrow 4s\ (3/2)_{5,2,1}$	2.6, 1.2×10^{-7}	706.7, 738.4	13.3	7800	0.002
$4p'(3/2)_2 \rightarrow 4s\ (1/2)_1$	4.5×10^{-8}	840.8			
$4p'(1/2)_1 \rightarrow 4s\ (1/2)_1$	6.5×10^{-8}	826.5	13.33	19,000	0.001
$4p'(1/2)_1 \rightarrow 4s\ (3/2)_2$	1.6×10^{-7}	696.5	13.33		
$4p'(1/2)_0 \rightarrow 4s'\ (3/2)_2$	1.6×10^{-7}	696.5	13.33		
$4p'(1/2)_0 \rightarrow 4s'\ (1/2)_1$	2.2×10^{-8}	750.4	13.48	3100	0.004
$3d(1/2)_0$	forbidden		13.84	2600	0.005
$3d(1/2)_1 \rightarrow 1S_0$	allowed	894	13.86	63,000	0.0002
$3d(3/2)_2$	forbidden		13.9	2800	0.005
$3d(7/2)_4$	forbidden		13.98	3700	0.004
$3d(7/2)_3$	forbidden		14.01	8600	0.002
$3d(5/2)_2$+ $5s(3/2)_2$	forbidden		14.07	6900	0.002
$5s(3/2)_1$	allowed		14.09	2700	0.005
$3d(3/2)_1 \rightarrow 1S_0$	3.2×10^{-9}	86.7	14.3	720	0.019
$4d(1/2)_1$	allowed		14.71	27,000	0.005
$6s(3/2)_1$	allowed		14.85	6100	0.002
$4d(3/2)_1$	allowed		14.86	2400	0.006
$4d'(3/2)_1$	allowed		15.0	2700	0.006
$6s(1/2)_1$	allowed		15.02	6600	0.002
$5d(1/2)_1$	allowed		15.12	20,000	0.001
$7s(3/2)_1$	allowed		15.185	7000	0.002
$5d(3/2)_1$	allowed		15.189	3000	0.005
$6d(1/2)_1$	allowed		15.31	120,000	0.0001
$6d(3/2)_1$	allowed		15.349	3200	0.005
$5d'(3/2)_1$	allowed		15.35	180,000	8.53e-5
$7s(1/2)_1 \rightarrow 4p(3/2)_2$	1.1×10^{-6}	602.5	15.36	130,000	0.0001
$8s(3/2)_1 \rightarrow 4p(3/2)_1$	6.7×10^{-6}	594.9	15.37	71,000	0.0002
$7d(1/2)_1$+…	allowed		15.66	890	0.018

Table IV. Theoretical results for N_2=O_2=Ar: (ε_0 = 30 eV) for an initial beam energy of 2 keV

	Excitation energy W_i (eV)	Mean energy per state ε_i (eV)	Mean energy per state ε_i (eV) pure gases
Major allowed			
$B^3\Sigma$ (N_2^+)	18.8	330	310
$b^4\Sigma$ (O_2^+)	18.2	250	240
$4s(3/2)_1$ (Ar)	11.62	560	480
$4s'(1/2)_1$ (Ar)	11.83	140	140
$3d'(3/2)_1$ (Ar)	14.3	580	720
Major forbidden			
$C^3\Pi$ (N_2)	11.00	450	620
$4s(3/2)_2$ (Ar)	11.55	2200	680
$4s'(1/2)_0$ (Ar)	11.72	11,500	5600

Table I indicates that roughly one-sixth of the molecular nitrogen ions are born in the $B^2\Sigma$ state, making the second positive system ($B^2\Sigma \rightarrow X^2\Sigma$) a strong radiator. Moreover, while all neutral excited states listed in Table I are metastables (i.e., those below 12.85 eV), roughly three times as many ions in total are produced as metastables. In contrast to other metastables, the $C^3\Pi$ state has a natural lifetime of only 45 ns, comparable to that of optically allowed states. The $C^3\Pi$ state thus radiates strongly at 337 nm, although not as strongly as the $B^2\Sigma$ ion at 391 nm.

Similarly, in oxygen (Table II), nearly three-times as many ions are produced as high-lying excited neutrals. However, in this case the strongest emission is predicted to be the neutral transition, $B^3\Sigma \rightarrow X^3\Sigma$. The production efficiencies for states with excitation energies below 5 eV are not listed for the reasons given earlier.

ii. Argon

Argon lacks excited states below 11.55 eV and thus below this energy, elastic collisions are the only electron cooling mechanism. However, PLUME does not incorporate elastic cooling, and so the electrons never stop traveling if the cutoff energy is less than 11.55 eV. To circumvent this problem, the cutoff energy was raised to 11.6 eV, just below the threshold of the next excited state. Electrons with energies between 11.55 and 11.6 eV can still produce the lowest excited state, and that contribution is estimated to be ~ 5% (as indicated by the asterisk in Table III).

According to Table 3, the brightest argon line in the wavelength range 700 - 970 nm occurs at 750.4 nm. The emission at 104.8 and 106.7 nm is much brighter yet, but those lines lie outside the range of the spectrometer used in the experiments. The energies of those photons exceed 11 eV, enough to modify the material's chemistry and morphology.

iii. Mixtures (N_2=O_2=Ar)

To assess the sensitivity of the mean electron energies to gas composition, the code was run in a mixture containing equal amounts of argon, oxygen and nitrogen and a cut off energy of 5 eV. Table IV gives ε_i (eV) for key states. The values of ε_i (eV) in pure gases is shown as

reference. Note that the mean energy per state in mixtures changes by less than 20 % for allowed states ($3d'(3/2)_1$ Ar exception) but by considerably more for the forbidden states.

e) ***Metastables***

Based on the efficiencies listed in Tables I-IV, ionization consumes nearly half the energy deposited by electron beams, with the rest of the energy being spent on the production of optically allowed states, forbidden states (metastables), and dissociation. Most metastables have long lifetimes, and thus the metastable population can grow to high levels. Metastables have little effect on beam-produced plasmas, as long as the ground-state population is not seriously depleted. This requirement was well met in the present experiments, as shown below.

The mean lifetime of a metastable is given by $\tau_m = (\tau_i^{-1} + \tau_d^{-1} + \tau_r^{-1} + \tau_q^{-1})^{-1}$, where τ_i is the radiative lifetime, τ_d is the diffusion time, τ_r is the residence time in the chamber due to pumping, and τ_q is the quenching time. If τ_+ is the mean ion lifetime and ε_m is the mean energy needed to create a metastable, the population of metastables relative to that of ions is given in steady state by $N_m/N_+ = (\varepsilon_0 \tau_m / \varepsilon_m \tau_+)$. This equation applies to any state, and for all states $\varepsilon_i > \varepsilon_0$ as shown by the tables. For example, consider argon at room temperature and low pressure. In that case $\varepsilon_0 \cong 27$ eV, $\varepsilon_m \cong 140$ eV for the major state $4s'(1/2)_1$, and the gas temperature $T_0 \cong T_e/40$. Diffusion determines the lifetime of both ions and metastables, so that $\tau_m / \tau_+ \cong D_a / D_m \cong T_e / T_0 \cong 40$. Here D_a is the ambipolar diffusion coefficient for ions, and D_m is the diffusion coefficient for metastables. Thus beam-produced plasmas in argon contain approximately ten times as many metastables as ions. The ratio can be even larger in molecular gas like nitrogen, where the electron-ion recombination reactions rapidly destroy the molecular ions. In the experiments reported, the ion density was always several orders of magnitude below the neutral density, which suggests that the gas remained weakly perturbed. It should be noted that the preceding calculation ignores metastables produced by the decay of higher-lying states. Including this contribution is simple but messy, and it will not effect the results significantly.

f) ***Model validation***

The values listed for ε_i in nitrogen and oxygen agree well with those computed by Konovalov,[36] and similar agreement is seen for much of the emission data, as discussed above. Bretagne et al. used the continuous-slowing-down approximation to model beams in argon. This approach is less accurate than the Monte Carlo scheme used in PLUME, but the two models should yield similar values for ε_i. However, while the values for ε_0 agree well, the values of ε_i for states other than ionization differ by nearly a factor of two. Bretagne's values appear to be in error, because they suggest that the lowest mean energy of the plasma electrons is close to 11.55 eV, whereas in fact it should be roughly half that large. The reason for the error is unknown.

The mean energy needed to produce an ion has been measured by many researchers, and thus it is a convenient test for the code. For nitrogen, the experimental and theoretical values are essentially identical at 36 eV. The agreement is almost as good in argon, 27 eV from the code versus 26 eV from experiment,[37] and the agreement was even better using Hayashi's cross sections. In oxygen the code gave ε_0 = 28 eV as compared with 31 eV from experiment. (Konovalov predicted 36 eV.) The discrepancy between PLUME and experiment suggests either that the ionization cross section used in PLUME is too large, or that one or more of the inelastic cross sections is too small.

4. Experimental method

a) *Optical emission spectroscopy measurements*

Emission spectra were taken using a wide band, low resolution spectrometer (Ocean Optics, HR 2000). The light emitted from the plasma is collected on a spherical mirror and then sent to a plane grating. The diffracted light is focused again by a second spherical mirror, and an image of the spectrum is projected onto a linear CCD array. Data from the CCD is transferred to a computer through an onboard A/D converter and analyzed using SpectraSuite software. The wavelength range was from 200 to 1100 nm (6.2 to 1.2 eV). For all experiments, the spectra were taken with a constant integration time of 1 second, the recorded data was averaged over 20 spectra, and the only applied correction was for electrical dark signal. In all cases, the following data collection procedure was followed: first a spectrum with no plasma was taken, then at the desired plasma conditions a spectrum was acquired, and finally the difference between the two spectra was used for analysis.

b) *Electron beam plasma system descriptions and operating conditions*

The experimental apparatus has been discussed previously[38] and is shown in the schematic of Figure 4. The system vacuum was maintained by a 250 l/s turbo pump, with a base pressure on the order of 5×10^{-6} Torr. The operating pressure was achieved by introducing argon (purity > 99.9999 %), nitrogen (purity > 99.99 %) and oxygen (purity > 99.99 %) through mass flow controllers and throttling the turbo pump using a manual gate valve. The electron beam was produced by applying a 2 kV pulse to a linear hollow cathode for a selected pulse width and duty factor. The emergent beam passed through a slot in a grounded anode and was then terminated at a second grounded anode located further downstream. The electrode beam volume between the two anodes defines the ionization source volume, with the dimensions set by the slot size (1 cm x 25 cm) and the anode-to-anode length (40 cm). Beam spreading from collisions with the background gas was suppressed by a co-axial magnetic field (150 G) produced by a set of external magnetic field coils. In all cases, a stainless-steel stage 10.2 cm in diameter was located at 2.5 cm from the edge of the electron beam. In a few cases, polystyrene samples were positioned on top of the stage. Because the beam is collimated, few high energy electrons strike the stage. The stage was grounded and at room temperature.

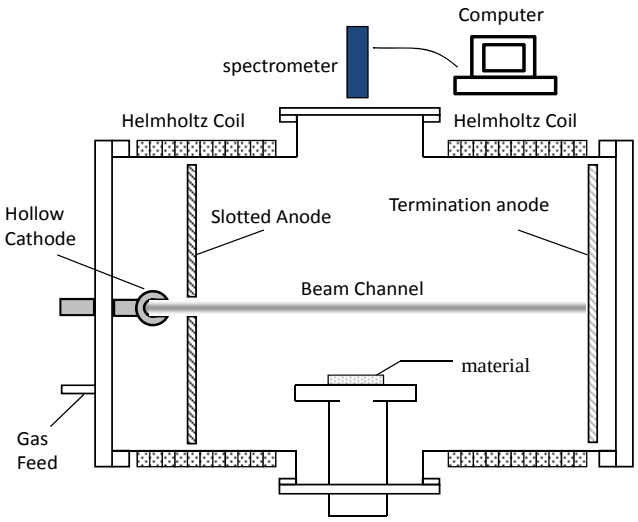

Figure 4. Schematic of the experimental setup

Optical emission spectra of electron beam generated plasma in different gas environments were acquired. Table V summarizes the experimental conditions for pure gases - argon, oxygen and nitrogen. The influence of pressure and duty factor on the emission intensity was studied experimentally. Table VI presents the experimental conditions for Ar/O_2 and Ar/ N_2 mixtures at a constant pressure and duty factor.

Table V. Experimental conditions for pure gases.

Gas	Pressure (mTorr)	Duty (%)	Notes
Argon	35	10	
	50	10	Polymer present
	50	20	
	50	40	
	75	10	
	90	10	
Nitrogen	35	40	
	50	20	
	50	40	Polymer present
	70	40	
Oxygen	35	10	
	50	10	Polymer present
	50	20	
	50	40	
	70	10	

Table VI. Experimental conditions in Ar/O_2 and Ar/N_2 mixtures. Pressure of 50 mTorr and duty factor (20 % for Ar/O_2 and 40 % for Ar/N_2 mixtures) was held constant.

Oxygen/Nitrogen flow (sccm)	Argon flow (sccm)
0	50
5	45
15	35
25	25
35	15
45	5
50	0

5. Experimental results

a) *Emission spectra*

i. Nitrogen

The emission spectrum measured in pure nitrogen at 70 mTorr is shown in Figure 5. Excited molecular and singly charged ions, excited nitrogen atoms and molecules were detected. A simplified energy diagram is presented in Figure 6.

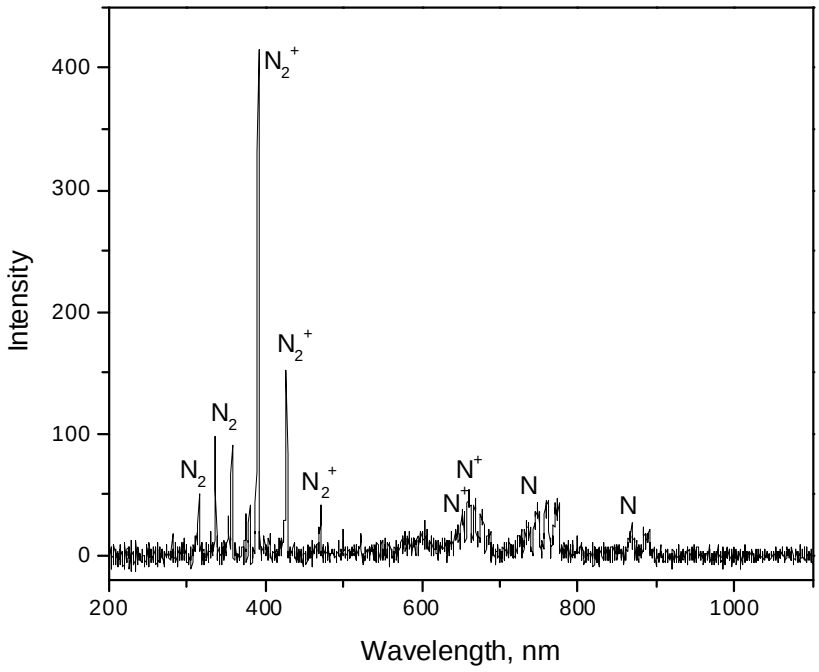

Figure 5. Emission spectrum in nitrogen at pressure of 70mTorr and 40 % duty factor.

The dominant emission was the band emission of the molecular nitrogen ion from the first negative system N_2^+ ($B^2\Sigma_u^+ \rightarrow X^2\Sigma_g^+$) with dominant emission line at λ = 391.44 nm. This result is in excellent agreement with the theoretical predictions (Table I) and suggests that the direct excitation and ionization reaction,

$$e + N_2 \rightarrow (N_2^+)^* + e,$$

is dominant for electron beam generated plasmas. Due to the high energy threshold for this reaction (E_{th} = 18.8 eV), high energy electrons are the main contributors to the molecular ions production and thus this emission line can be used for electron beam diagnostics.

Direct excitation of neutrals,

$$e + N_2 \rightarrow N_2^* + e,$$

is the second dominant process. In particular, band emissions from the first-positive ($B^3\Pi_g \rightarrow A^3\Sigma_u^+$, E_{th} = 7.35 eV) and the second-positive ($C^3\Pi_u \rightarrow B^3\Pi_g$, E_{th} = 11 eV) systems were detected. The threshold levels for excitation are much lower than for the charged species, and thus the influence of low energy electrons on their production is more significant. Therefore, these emission lines are less useful as a beam diagnostics tool.

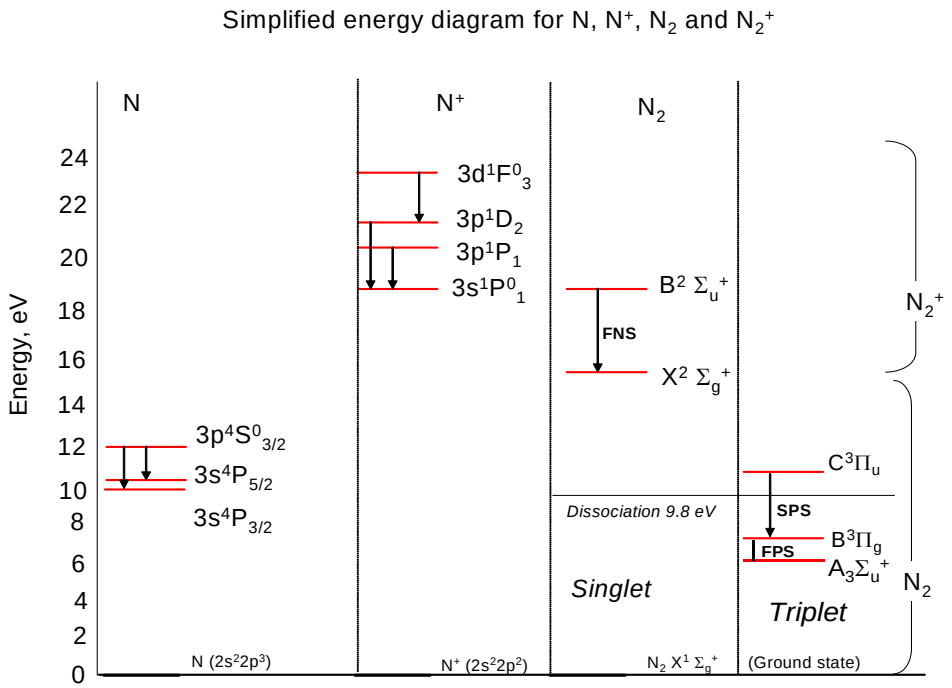

Figure 6. Simplified energy diagram for excited species in nitrogen. The acronyms FNS, FPS, SPS denote first negative, first positive and second positive systems respectively.

Excited singly charged atoms were also detected, with the most likely source being dissociative ionization and excitation,

$$e + N_2 \rightarrow (N^+)^* + N.$$

Because this process requires high threshold energies, only the beam electrons contribute significantly. Major transitions include $3p^1D_2$ to $3s^1P^0_1$ (λ = 399.5 nm, E_{th} = 21.6 eV), $3p^1P_1$ to $3s^1P^0_1$ (λ = 648 nm, E_{th} = 20.4 eV), $3d^1F^0_3$ to $3p^1D_2$ (λ = 661 nm, E_{th} = 23.5 eV), $3p^3S^0_1$ to $3s^3P_1$ (λ = 885.5 nm, E_{th} = 27.7 eV), and from $5s^3P^0_2$ to $4p^3P_1$ (λ = 894 nm, E_{th} = 26.6 eV). However, the emission from excited atomic ions was weak compared with that from excited molecular ions, $I_{N+}(661\text{ nm}) \cong 0.12 I_{N2+}(391\text{ nm})$.

Major emissions for the excited nitrogen atoms included transitions from $3p^4S^0_{3/2}$ to $3s^4P_{3/2}$ (λ = 744 nm, E_{th} = 12 eV), $3p^4S^0_{3/2}$ to $3s^4P_{5/2}$ (λ = 746.8 nm, E_{th} = 12 eV), and from $3p^4D^0_{7/2}$ to $3s^4P_{5/2}$ (λ = 868.03 nm, E_{th} = 11.8 eV). This emission arose either through dissociation and excitation,

$$e + N_2 \rightarrow e + N^* + N,$$

or more likely through dissociative recombination,

$$e + N_2^+ \rightarrow N^* + N,$$

of molecular ions with plasma electrons. The peak emission from neutral atoms was less than that from neutral molecules, $I_N(746.9\text{ nm}) \cong 0.39 I_{N2}(358\text{ nm})$, and smaller yet compared with the emission from molecular ions. Equally important, virtually all of the $N_2^+(B^2\Sigma)$ ions in these experiments should have decayed to $N_2^+(X^2\Sigma)$ well before recombining with plasma electrons, since the natural lifetime of $N_2^+(B^2\Sigma)$ is only 66 ns while the rate coefficient for dissociative recombination is less than 10^{-7} cm^3/s and $n_e < 10^{12}$ cm^{-3}.

ii. Oxygen

In oxygen, emissions from excited atoms, molecular ions, and atomic ions (at the highest pressure) were detected, as shown in Figure 7. A simplified energy level diagram for the oxygen atom, atomic ion, and molecule is shown in Figure 8. The transitions for the most intense lines are shown as well.

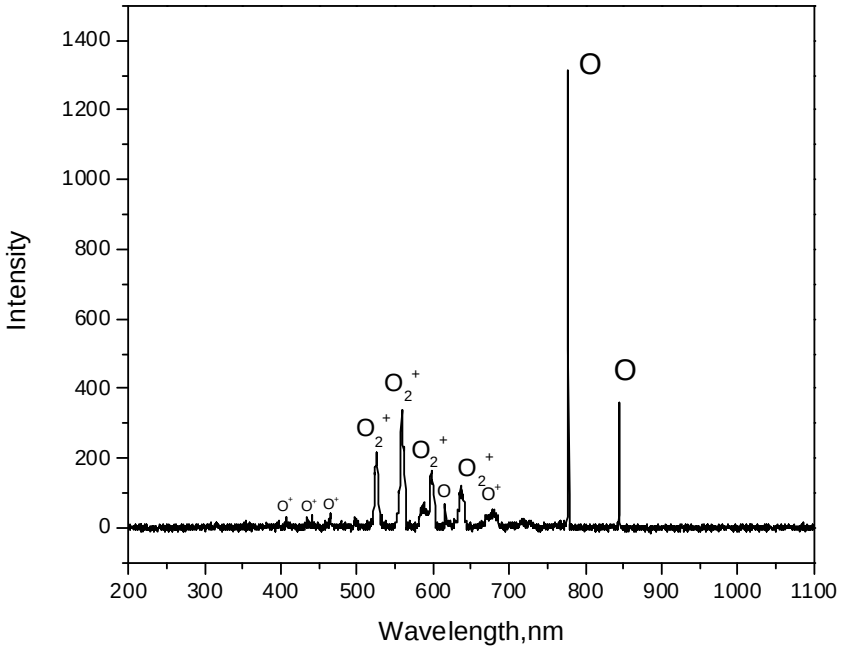

Figure 7. Emission spectrum in oxygen at a pressure of 70 mTorr and a duty factor of 20 % duty.

The emission spectrum shows bands of oxygen molecular ions produced by direct excitation and ionization,

$$e + O_2 \rightarrow (O_2^+)^* + e.$$

This emission arose predominantly from the first negative system ($b_4\sum_g^- - a_4\Pi_u$) (λ = 559 nm, 525 nm) and is in qualitative agreement with the predictions of PLUME. However, the strongest emission came from excited neutral atoms and is associated mainly with transitions between $3p^5P$-$3s^5S^0$ (λ = 777.19 nm), $3p^3P$-$3s^3S^0$ (λ = 844.67 nm), and $4d^5D^0$-$3p^5P$ (λ = 615.59 nm). This emission presumably arose from dissociative excitation

$$e + O_2^+ \rightarrow O^* + O,$$

a process not included in PLUME. Since the production of O* depends quadratically on the plasma density, the emission from O* is strong only if the plasma density is sufficiently high. The emission ratio for O(777 nm)/O_2^+(559 nm) thus varies with pressure, equaling 3.9 at p = 70 mTorr. These results suggest that the emission from O_2^+ can be used to infer the rate of beam energy deposition in oxygen, while the emission from O* can be used to infer the loss of O_2^+ to recombination.

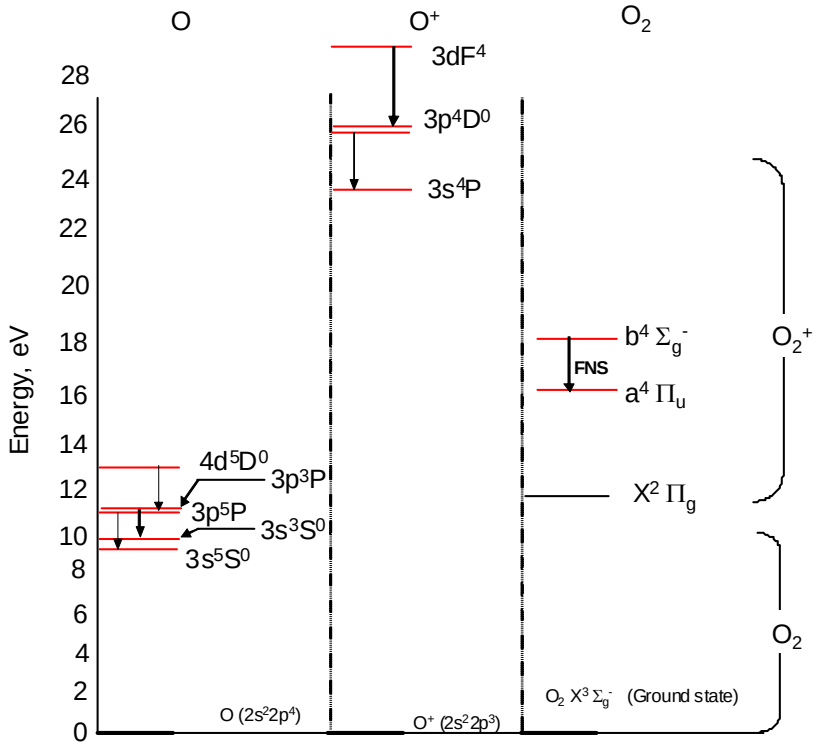

Figure 8. Simplified diagram for excited species in oxygen. The acronym FNS denote first negative system.

PLUME indicates that almost as many $B^3\Sigma$ molecular oxygen neutrals are created as ions ($\varepsilon_i \cong 42$ eV versus $\varepsilon_0 \cong 28$ eV), but this state dissociates (~ 0.05 ns) long before it radiates (~ 500 ns). Thus it is not surprising that no excited oxygen molecules were detected. For the excited

atomic ions, two predominate transitions were detected: $3d^4F\text{-}3p^4D^0$ (λ = 407.59 nm) and $3p^4D\text{-}3s^4P$ (λ = 464.18 nm). These excited ions are produced by the beam through dissociative ionization and excitation,

$$e + O_2 \rightarrow (O^+)^* + O.$$

In these experiments, the intensity ratio O^+(464.18 nm)/O_2^+(559 nm) ≅ 0.12.

iii. Argon

Emission from excited neutral atoms (Figure 9) was predominant in argon. Some of these transitions are shown in the simplified energy level diagram in Figure 10 using Racah, Paschen and L-S notations. The optical emission measured by the spectrometer comes mainly from depopulation of the 4p levels via multiple 4p-4s transitions, including $4p(5/2)_3 \rightarrow 4s(3/2)_2$ for λ = 811.5 nm, $4p(3/2)_2 \rightarrow 4s(1/2)_{1,2}$ for λ = 763.5 nm and 922.4 nm, $4p(5/2)_2 \rightarrow 4s(3/2)_{1,2}$ for λ = 801.5 nm and 842.5 nm, $4p(3/2)_1 \rightarrow 4s(3/2)_{1,2}$ for λ = 810.4 nm and 772.4 nm , $4p'(1/2)_0 \rightarrow 4s'(1/2)_1$ for λ = 750.4 nm. Emission from atomic ions was evident only at the highest pressure used, 90 mTorr.

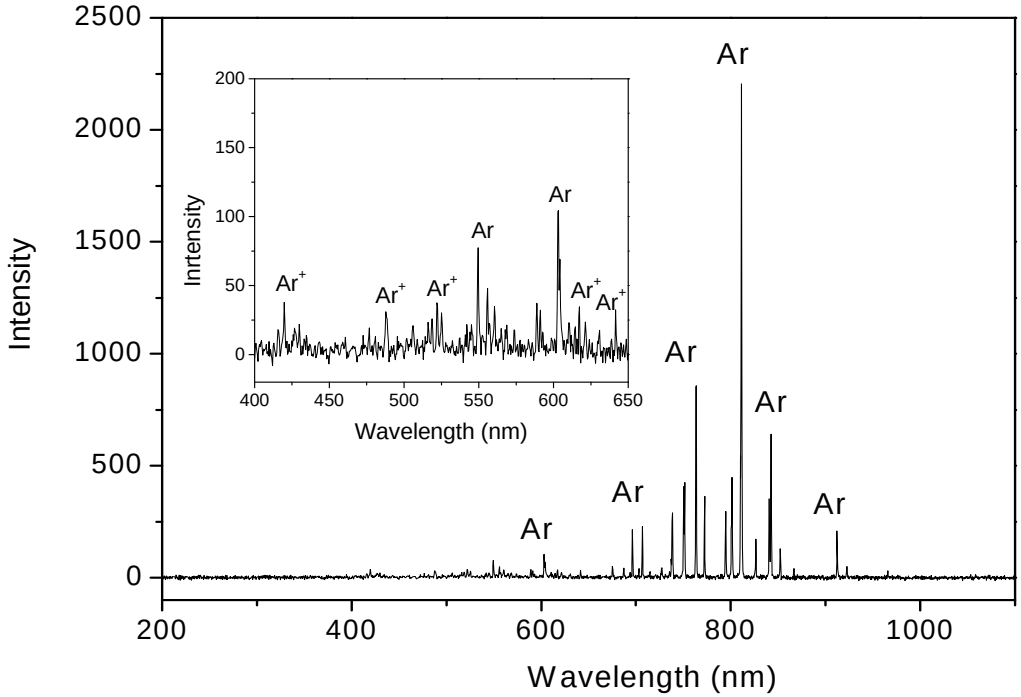

Figure 9. Emission spectrum in argon at a pressure of 90 mTorr and 10% duty factor.

The line ratios in the 700-900 nm range agreed qualitatively but not quantitatively with the predictions from PLUME. In particular, PLUME indicates that the 750.45 nm line should be dominant, whereas experimentally the 811.5 nm line was the most intense. However, neither the 811.5 nm line nor the 750.45 nm line is ideal as a beam diagnostic, since both lines result from the decay of metastables. Accordingly, the production of these states is more affected by the low-energy tail of the energy distribution than is the production of optically allowed states which

as mentioned before are mainly produced by high energy electrons and thus ideally suited for electron beam diagnostics.

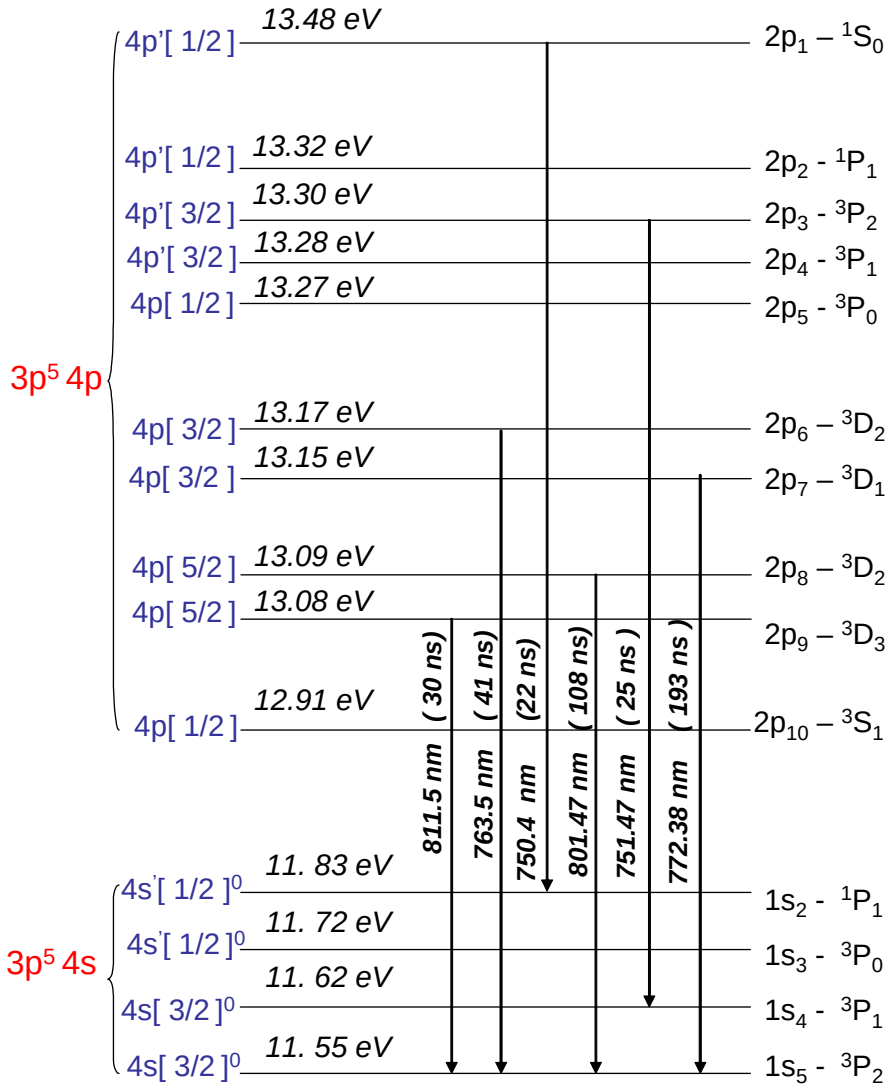

Figure 10. Simplified energy diagram for excited argon atom transitions. In the literature three different notations have been used to describe the same energy levels. For clarity all of them are shown - on the left is energy levels classification is based on Racah notation, on the right- on Paschen notation (1st column) and L-S notation (2nd column) respectively .

b) ***Effect of processing parameters on emission intensity ratios***

i. Duty factor and pressure

The light detected by the spectrometer comes from electronic states excited by the beam, with the excitation rates determined largely by the gas and the beam current and energy. In these experiments the gas was the same in the electron gun and in the chamber where the measurements were taken, and therefore the beam current depends on the gas composition. The highest current density was measured in oxygen, followed by argon and nitrogen (Figure 11). The current density also increased with pressure independent of the gas. Thus with pressure both the current and the plasma density increase. These two parameters affect the electron energy distribution and density at low energy, thus changing the emission intensities and in some cases the line ratios. For example, in Figure 12b the emission ratios for O/O_2^+ increased with increasing pressure. This increase was presumably caused by the increase in plasma density and higher rate of dissociative recombination. In Figure 12c the ratio Ar(811.5 nm)/Ar(750.45 nm) increased with pressure as well. However, in this case the increase was most likely caused by changes in the electron energy distribution. In nitrogen the line ratios were nearly independent of pressure, as shown in Figure 12a. Emission from these lines was thus governed more by the high-energy portion of the electron energy distribution.

Increasing the duty factor of the pulsed electron beam increases the time the beam is on, thus increasing the time-averaged emission emitted from a given gas; see Tables VII-IX. However, as expected, the duty factor did not significantly affect the *relative* intensities seen in Figure 13. To investigate the influence of a nearby insulator, polystyrene was mounted on a stainless-steel stage placed 2.5 cm outside the beam. The stage was positioned opposite the spectrometer as illustrated in Figure 4. Results with (+) and without (-) polystyrene are shown in Figure 12c. For all four investigated pressures, the intensity ratio decreased when polymer was present. The decrease was likely caused by photon absorption within the polystyrene, as compared with reflection from the stainless steel.

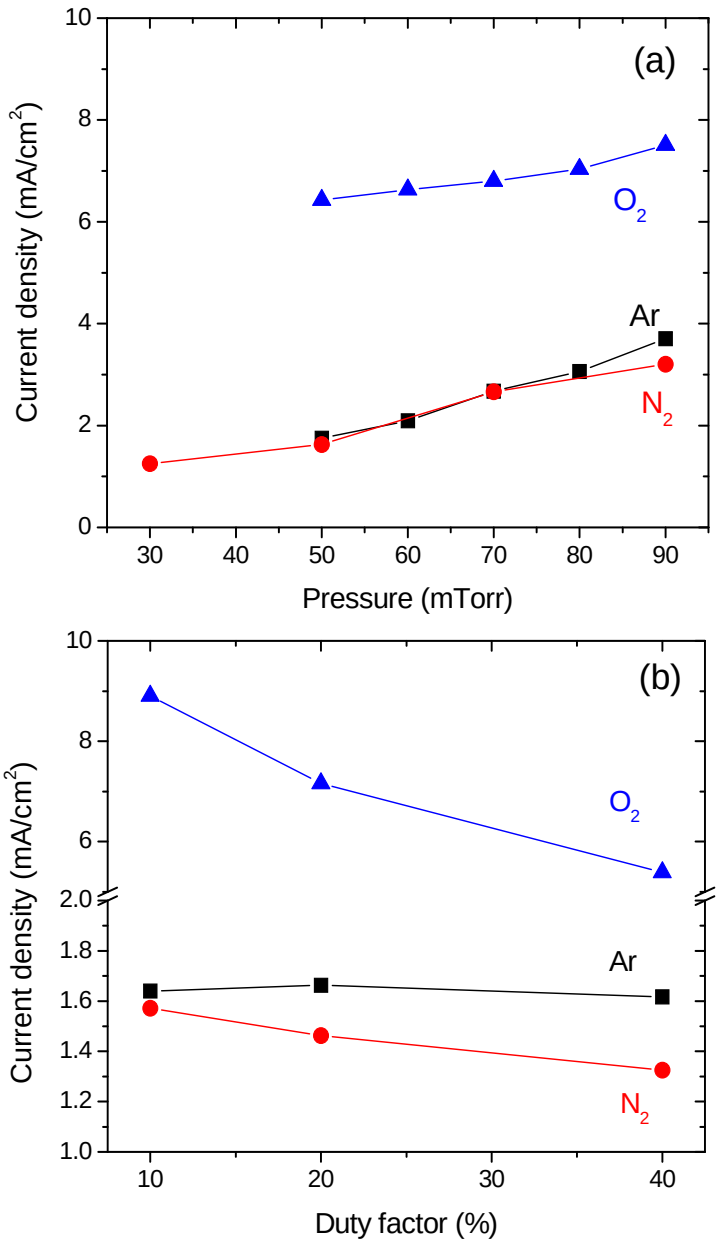

Figure 11. Effect of pressure (a) and duty factor (b) on the current density in argon, nitrogen and oxygen.

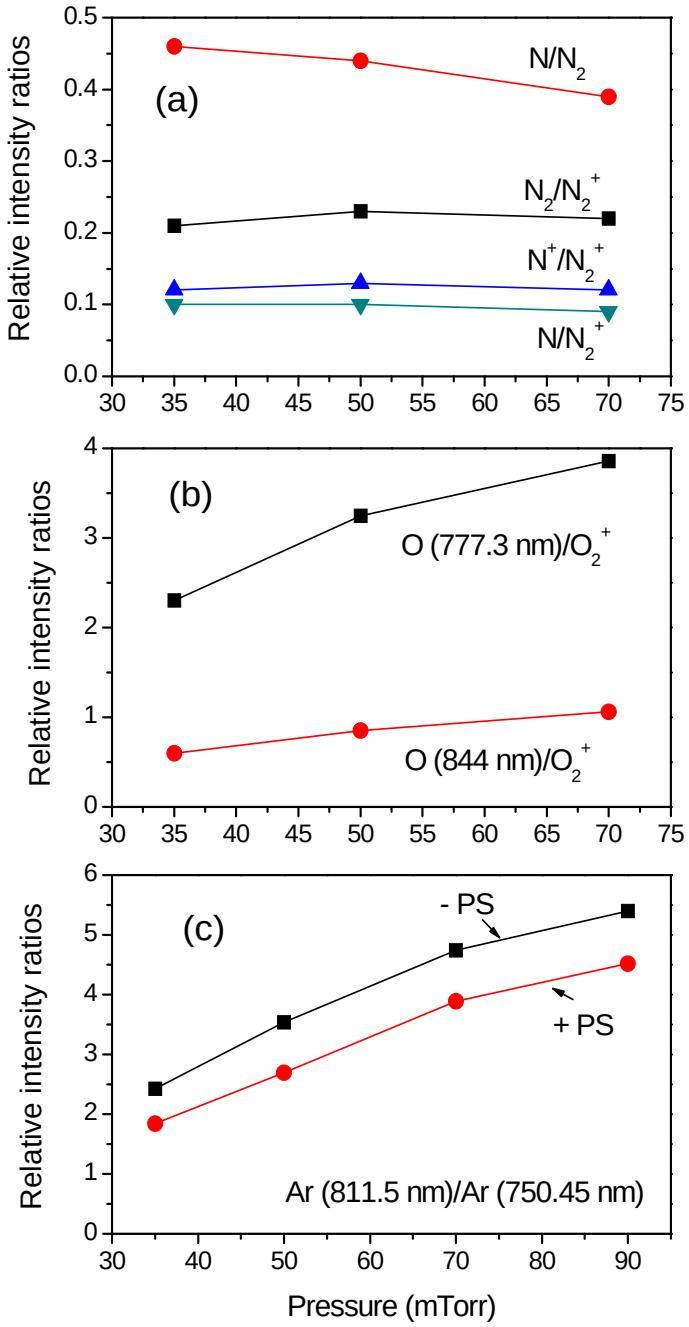

Figure 12. Effect of pressure on the relative intensity ratios in nitrogen (a), oxygen (b) and argon (c). For nitrogen (Fig. 12 a) the following wavelengths for the respective excited states were used: 746.9 nm (N*), 661.23 nm (N^+)*, 391.16 nm (N_2^+)*, 357.79 nm (N_2)*. The last wavelength was chosen because it had the highest intensity in the second positive system band. For oxygen (Fig. 12 c), the excited oxygen ion (O_2^+) was detected at 559 nm. For argon (Fig. 12 c) the labels (-PS) and (+PS) refer to experiments when polystyrene was not present on or present on the stage respectively.

Table VII. Summary of nitrogen lines intensities.

Wavelength, nm	Experimental conditions			
	P = 35 mTorr	P = 50 mTorr	P = 50 mTorr	P = 75 mTorr
	Duty = 40 %	Duty = 20 %	Duty = 40 %	Duty = 40 %
391.16 (N_2^+)	148.23	242.42	415.45	909.83
427.81 (N_2^+)	58.53	96.02	151.6	326.08
337.13 (N_2)	17.43	39.67	54.55	123.38
357.79 (N_2)	32.93	50.67	91.45	200.13
661.23 (N^+)	18.48	28.67	53.35	106.18
746.9 (N)	14.53	27.32	42.8	78.03

Table VIII. Summary of oxygen lines intensities.

Wavelength, nm	Experimental conditions				
	P = 35 mTorr	P = 50 mTorr	P = 50 mTorr	P = 50 mTorr	P = 75 mTorr
	Duty = 10 %	Duty = 10 %	Duty = 20 %	Duty = 40 %	Duty = 10 %
559 (O2+)	110.12	226.44	301.12	462.04	339.38
525 (O2+)	68.37	130.64	183.27	285.89	205.88
777.2 (O)	253.67	767.99	931.97	1402.69	1311.08
844.7 (O)	65.67	198.59	258.07	374.19	360.28

Table IX. Summary of argon lines intensities.

Wavelength, nm	Experimental conditions					
	P = 35 mTorr	P = 50 mTorr	P = 50 mTorr	P = 50 mTorr	P = 70 mTorr	P = 90 mTorr
Ar I	Duty = 10 %	Duty = 10 %	Duty = 20 %	Duty = 40 %	Duty = 10 %	Duty = 10 %
811.5	131.91	332.76	641	1143.95	1236.83	2204.84
763.5	49.56	142.41	282.8	516.35	499.38	857.64
842.46	44.16	98.66	196.8	378	372.08	640.74
801.47	33.31	70.26	138.45	249.8	254.98	448.84
750.45	54.31	94.01	188.4	366.65	260.78	408.34

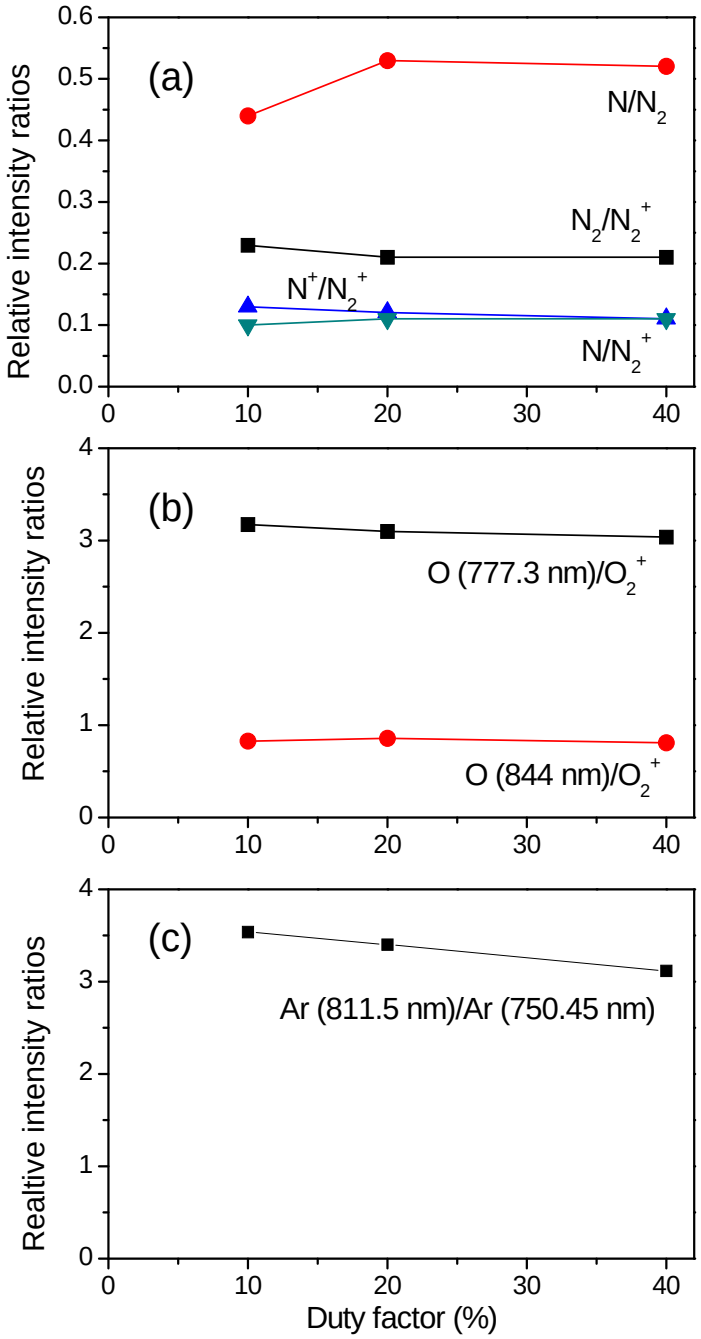

Figure 13. Effect of duty factor on the relative intensity ratios in nitrogen (a), oxygen (b) and argon (c). For nitrogen (Fig. 13a) the following wavelengths for the respective excited states were used: 746.9 nm (N*), 661.23 nm (N^+)*, 391.16 nm (N_2^+)*, 357.79 nm (N_2)*. The last wavelength was chosen because it had the highest intensity in the second positive system band. For oxygen (Fig. 13b), the excited oxygen ion (O_2^+) was detected at 559 nm.

ii. Effect of gas composition

Figure 14 shows the emission spectra in 50/50 mixtures of Ar/N_2 and Ar/O_2. The major lines represent light emitted by excited molecular ions (N_2^+, O_2^+), molecules (N_2), neutrals (Ar, O, N), and singly charged ions (N^+, O^+). In Ar/N_2 mixtures the dominant emission is from excited molecular nitrogen ions at λ = 391.1 nm and excited argon atoms at λ = 750.4 nm. Strong lines in Ar/O_2 mixtures include emission from excited Ar neutrals at λ = 750.4 nm, oxygen atoms at λ = 777.3 nm, and oxygen molecular ions at λ = 559.6 nm.

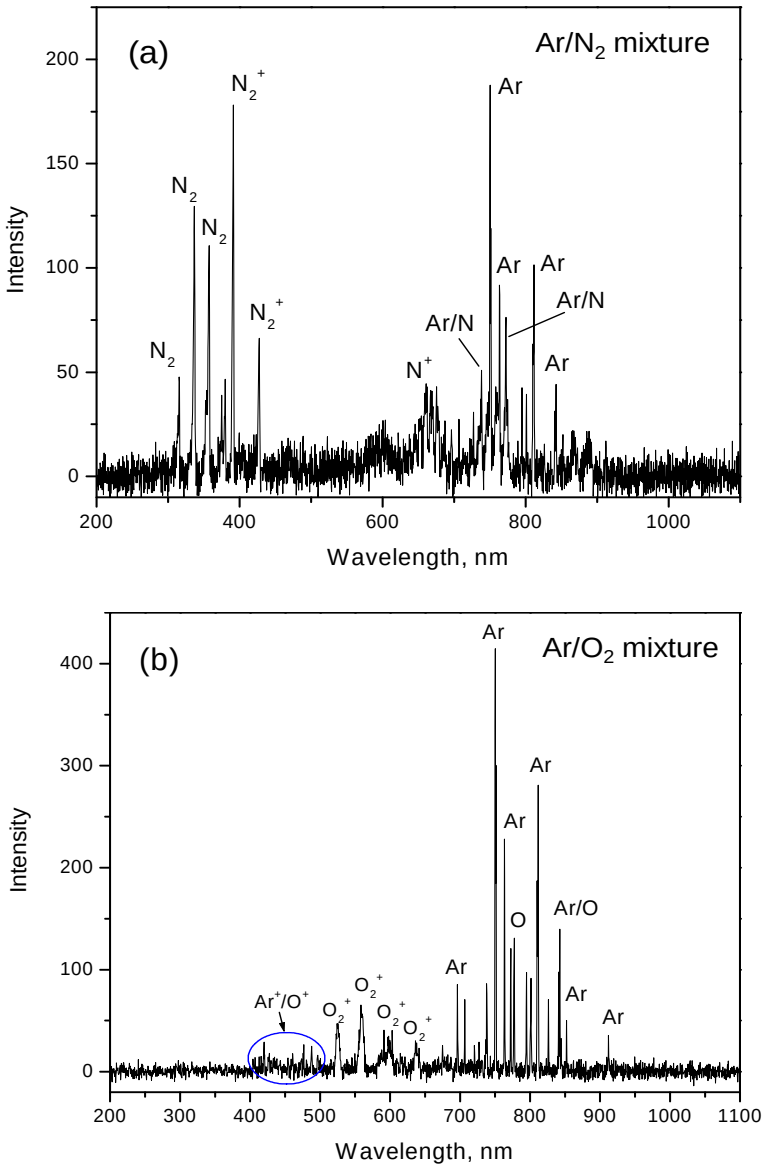

Figure 14. Emission spectra in a Ar/N_2 (50/50 by flow) (a) and Ar/O_2 (50/50 by flow) (b) mixtures.

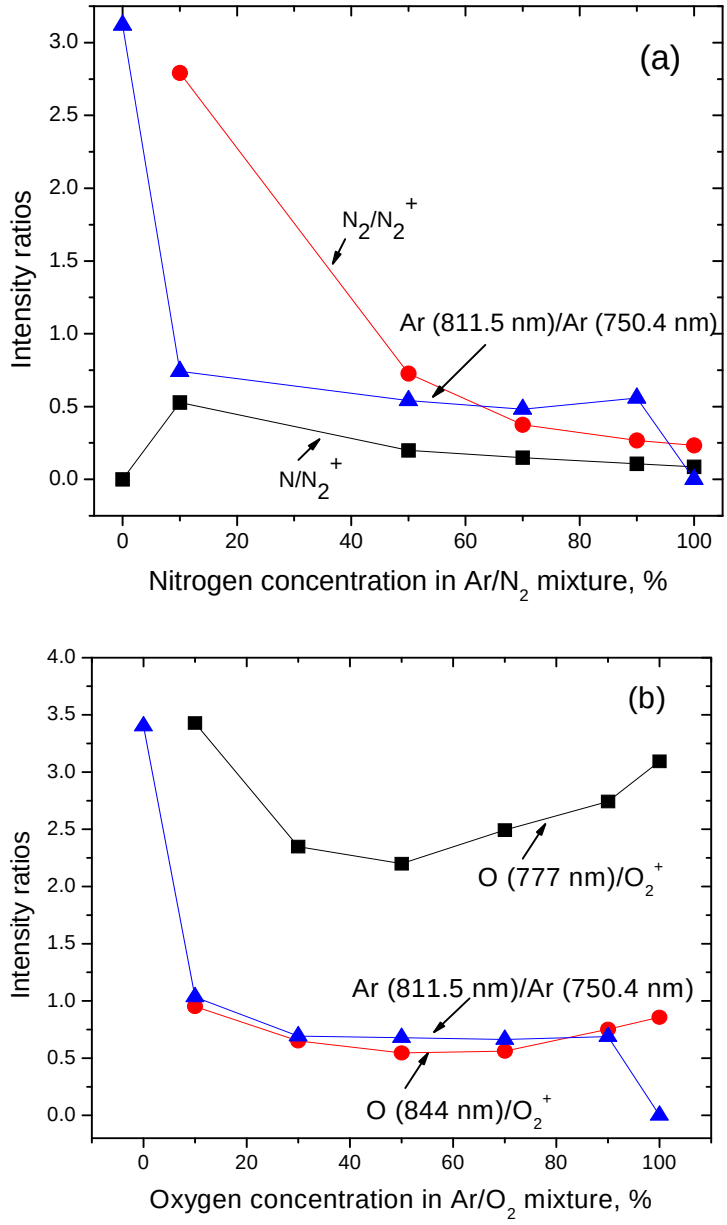

Figure 15. Dependence of the relative emission intensity ratios on the gas composition.

For both Ar/O_2 and Ar/N_2 mixtures, the observed molecular ions and argon neutrals were in qualitative agreement with the code. The shift in the dominant argon emission from 811.5 nm to 750.45 nm presumably occurs because of changes in the electron energy distribution. In particular, dissociative recombination with molecular ions rapidly removes low-energy electrons, such that the low-energy portion of the electron energy distribution is depressed when nitrogen or oxygen is added to Ar. Since production of the 811.5 nm line is sensitive to low-energy electrons, the ratio Ar(811.5 nm)/Ar(750.45 nm) is lower in the mixtures than in pure Ar. Figures 15a and b show several intensity ratios as a function of gas composition. The ratio Ar(811.5 nm)/Ar(750.4 nm) is largest in pure argon but fell by a factor of four when mixed with N_2 and by a factor of three when mixed with O_2. The ratio remained approximately constant for nitrogen

concentrations between 10 and 90 % and for oxygen concentrations between 30 and 90 %. Similarly, the low-energy portion of the electron energy distribution affects the nitrogen metastable $N_2(C^3\Pi)$ more than the ion $N_2^+(B^2\Sigma)$, and therefore the ratio N_2(337.1 nm)/N_2^+(391.4 nm) again fell with increasing nitrogen concentration in Figure 15a. The ratio O(777 nm)/O_2^+(559 nm) has a more complicated dependence on oxygen concentration in Figure 15b, presumably because of the interplay between changes in the electron energy distribution and the production of O* through recombination. The relative emission intensities of different lines in Ar/N_2 and Ar/O_2 mixtures are summarized in Tables X and XI respectively.

Table X. Summary of Ar/N_2 lines intensities (P = 50 mTorr, duty = 40 %).

Wavelength, nm	Experimental conditions(N_2/Ar flow ratios)				
	5/45	15/35	25/25	35/15	45/5
811.5 (Ar)	242.71	158.75	101.52	64.17	24.44
750.4 (Ar)	327.26	237.3	187.62	133.12	43.64
391.16 (N2+)	40.21	115.85	178.17	278.97	232.79
427.81 (N2+)	26.61	55.25	66.32	109.97	90.89
337.13 (N2)	63.56	73.45	74.12	75.42	32.14
357.79 (N2)	56.91	67.55	78.52	67.02	44.34
661.23 (N+)	35.06	38.8	36.92	41.87	32.79
746.9 (N)	18.31	26.5	29.97	33.07	22.34

Table XI. Summary of Ar/O_2 lines intensities (P = 50 mTorr, duty = 20 %).

Wavelength, nm	Experimental conditions (O_2/Ar flow ratios)				
	5/45	15/35	25/25	35/15	45/5
811.5 (Ar)	335.56	272.46	280.9	279.97	189.48
750.4 (Ar)	324.21	393.41	414.65	412.07	275.08
559 (O2+)	6.86	29.16	55	97.57	171.63
525 (O2+)	7.46	24.41	42.1	85.22	133.73
777.2 (O)	38.61	65.21	131	279.57	586.83
844.7 (O)	10.71	18.06	32.5	83.32	161.13

6. Comparison with other experiments

Optical emission spectroscopy has been applied for electron beam-generated plasma characterization at different gas environments. For example, Davidson and O'Neil[39] measured the light emitted by a 50-keV beam propagating in 600 torr of nitrogen and air. The brightest emission occurred at 391.4, 337.1, and 357.7 nm, where the latter two lines are part of the same band. However, because quenching strongly influences the emission at high pressure, Mitchell[40] measured the fluorescent efficiency for the dominant lines as a function of pressure. Quenching is weak at low pressure, and there the efficiencies approached 0.66% at 391.4 nm and 0.26% at 337.1 nm. These values correspond to mean energies of 480 and 1140 eV, respectfully. The ratio of these two values is close to that predicted by the code, but the absolute values are 50-80% larger. However, PLUME lumps all vibrational and rotational levels of a given electronic state together, even though the levels radiate at different frequencies. Therefore the mean energy for a given line within a band exceeds the mean energy for the band as a whole. Furthermore, experimental values typically vary by a factor of two,[41] similar to the uncertainty in the cross sections. Given these considerations, theory and experiment agree well for nitrogen.

Pu et al.[42, 43] applied optical emission spectroscopy to characterize electron beam-generated plasmas in argon and nitrogen. The obtained emission spectra in both gases agree very well with our data. The most intense line in argon and nitrogen are the 811 nm and 391 nm respectively. Furthermore, they applied collisional-radiative model and line-ratio method to estimate plasma and species densities and electron temperature. This will be subject of future work.

Attempts to compare our results with optical emission spectra obtained in discharges were made as well. However, given the difference in plasma generation, electron kinetics, metastable production etc., different OES spectra are expected.[44, 45] Furthermore, while some of the spectral differences are general in nature, others pertain to differences in condition. For example, the state of the gas in the discharges differed notably from that in our beam-produced-plasmas, even when the gas pressures and compositions were comparable. This is evident from estimates of the gas and vibrational temperatures and the degree of gas dissociation, excitation and ionization. The spectra should thus differ on that basis alone. Some of the fundamental differences between discharges and electron beam-generated plasmas are highlighted below.

When a high energy electron beam is applied to a gas, it ionizes, dissociates and excites the gas. No additional electric field is applied to keep the electrons hot, so they quickly lose their energy. The average electron energy is therefore low, usually less than 1 eV. In discharges, an external electric field is applied to heat the electrons, which in turn excite, dissociate and ionize the gas. In discharges the mean electron energy typically lies between 2 and 10 eV. In both cases the excitation, ionization and gas dissociation processes can be characterized in terms of the mean energy ε_i needed to create a given state. The mean energies are nearly constant for high energy beams[28] (> 1 kV) but not for discharges. For example, the electron energy ε_0 needed to create an electron–ion pair is 36 eV in nitrogen and 28 eV in oxygen. These values are slightly more than twice the ground state ionization energies, and thus approximately half of the beam energy is spent on ionization. Moreover, the mean energy is approximately 30 eV in all gases, independent of beam current and energy. In discharges, the mean energy varies strongly with the gas and plasma parameters, and often exceeds 1 keV. Thus the ionization efficiency is usually small (< 1 %), and most of the electron energy instead is spent on gas excitation and dissociation.

Furthermore, electron beam-generated plasmas and discharges produce different populations of excited species, and to demonstrate this let us compare results from several theoretical calculations. Ferreira et al.[46] determined that in argon, most of the power from a discharge is spent on producing metastables (as high as 40 %), followed by resonant states and elastic collisions; ionization becomes dominant only at very high field strengths. By contrast, electron beam-generated plasmas produce mostly ions, with roughly one metastable for every 11 ions[47]. Similarly, Slinker et. al.[48] computed the production efficiencies for both the primary (beam) electrons and the secondary low energy electrons created by ionization for electron beams propagating in nitrogen. The production efficiencies were computed for direct and dissociative ionization, inner shell processes, vibrational, triplet and singlet excitation and dissociation reactions. Those results again indicate that most of energy deposited by the beam electrons goes into ionization, with smaller amounts going into dissociation and excitation. The low energy electrons, by contrast, favor excitation. Of the 36 eV spent per electron-ion pair, 20.1 eV was spent on ionization, 13.3 eV was spent on producing N_2^+, and 6.8 eV on N^+. Production of N takes 6.69 eV. Excited species require an additional 7.78 eV, triplet states (3.83 eV), vibrational states (2.62 eV) and singlets (1.33 eV). The contributions of inner-shell processes (1.1 eV) and rotational excitation (0.41 eV) are negligible. Slinker et. al. also computed the deposition fraction of heat, rotational, vibrational, triplet and singlet excitations, dissociation and ionization reactions in nitrogen swarms as a function of the reduced electric field (E/N). At $E/N < 10^{-15}$ Vcm^2 vibrational excitation is the dominant mechanism, followed by triplet, singlet and, rotational excitation. At $E/N > 10^{-15}$ Vcm^2 triplet excitation is dominant, followed by singlet excitation, dissociation and ionization reactions.[28]

7. Conclusions

In this study optical emission spectroscopy was applied for characterization of electron beam-generated plasmas. The OES spectra provided information about the beam, the gas composition, and the electron kinetics, i.e. how quickly excited states have been generated and destroyed. Because most of the light is produced by the beam, OES spectra cannot be used directly for estimation of the electron temperature. However, when lines that come from one or more high-lying, optically allowed states with large cross section and short lifetimes are used, OES can be used as a beam diagnostic. Gas quenching and photon re-absorption should be weak as well. In conjunction with Abel inversion, OES can in principle be used to determine not only the species being generated but also the rate at which the beam deposits energy in the gas and thus the beam current density. The particular results based on the emission produced by electron beams in pure argon, nitrogen, oxygen, and Ar/N_2 and Ar/O_2 mixtures can be summarized as follows:

(1) In nitrogen, the dominant line (391.16 nm) came from an excited molecular ion. In oxygen, molecular ions were detected but the dominant emission (777.2 nm) came from an excited atom, presumably produced through dissociative recombination of plasma electrons with O_2^+. Argon ion lines were weak or nonexistent, but the brightest line (above 200 nm) came from an excited neutral at 811.5 nm.
(2) The effects of pressure, duty factor and presence of an insulator on the emission were analyzed as well. In the pulsed electron beam-produced plasmas studied here, independent control over beam current and pressure is not possible. Increasing the duty

factor increased the intensities but not the intensity ratios, as expected. However, with increasing gas pressure, the gas density, beam current, and plasma density all increase, and the emission ratios were then no longer constant. The presence of an insulator reduced the intensities, an effect attributed to different photon absorption coefficients in steel versus polystyrene.

(3) The best agreement between experiment and theory was obtained in pure nitrogen and Ar/N_2 mixtures. The use of the emission line at 391 nm as a beam diagnostic was clearly demonstrated. The agreement was slightly worse in argon, oxygen, and Ar/O_2 mixtures.

8. Acknowledgements

E. H. Lock would like to acknowledge I. Singer for letting her use the Ocean optics spectrometer.

9. References

1. J. C. Swartz, B. D. Guenther, F. C. D. Lucia, W. Guo, C. R. Jones, H. Kosai and J. M. Dutta, *Phys. Rev. E*, 1995, **52**, 5416-5424.
2. J. W. Elmer, A. T. Teruya and D. W. O'Brien, *Welding J.*, 1993, 493s-505-s.
3. R. E. Shefer, Y. Z. Yin and G. Bekefi, *J. Appl. Phys.*, 1983, **54**, 6154-6159.
4. T. J. Webb, K. D. Hahn, M. D. Johnston, B. V. Oliver and D. R. Welch, *IEEE Trans. Plasma Sci.*, 2010, **38**, 923-932.
5. M. Baraket, S. G. Walton, E. H. Lock, J. T. Robinson and F. K. Perkins, *Appl. Phys. Lett.*, 2010, **96**, 231501.
6. D. Leonhardt, C. Muratore and S. G. Walton, *IEEE Trans. Plasma Sci.*, 2005, **33**, 783-790.
7. E. H. Lock, D. Y. Petrovykh, P. Mack, T. Carney, R. G. White, S. G. Walton and R. F. Fernsler, *Langmuir*, 2010, **26**, 8857-8868.
8. S. G. Walton, C. Muratore, D. Leonhardt, R. F. Fernsler, D. D. Blackwell and R. A. Meger, *Surf. Coat. Technol.*, 2004, **186**, 40-46.
9. E. H. Lock, R. F. Fernsler and S. G. Walton, *Plasma Sources Sci. Technolog.*, 2008, **17**, 025009.
10. D. Leonhardt, S. G. Walton, D. D. Blackwell, W. E. Amatucci, D. P. Murphy, R. F. Fernsler and R. A. Meger, *J. Vac. Sci. Technol. A*, 2001, **19**, 1367-1373.
11. D. R. Boris, R. F. Fernsler and S. G. Walton, *Plasma Sources Sci. Technolog.*, 2011, **20**, 025003.
12. R. A. Gottscho and T. A. Miller, *Pure & Appl. Chem.*, 1984, **56**, 189-208.
13. J. M. Stillahn, K. J. Trevino and E. R. Fisher, *Annual Review Anal. Chem.*, 2008, **1**, 261-291.
14. S. P. Slinker, R. D. Taylor and A. W. Ali, *J. Appl. Phys.*, 1987, **63**, 1-10.
15. J. Bretagne, J. Godart and V. Puech, *J. Phys. D: Appl. Phys*, 1982, **15**, 2205-2225.
16. J. Bretagne, G. Callede, M. Legentil and V. Puech, *J. Phys. D: Appl. Phys*, 1986, **19**, 761-777.
17. J. Bretagne, G. Callede, M. Legentil and V. Puech, *J. Phys. D: Appl. Phys*, 1986, **19**, 779-793.
18. R. F. Fernsler, S. P. Slinker and S. G. Lambrakos, *J. Appl. Phys.*, 2008, **104**, 063312.

19. S. P. Khare and A. K. Jr, *J. Phys. B: Atom. Molec. Phys.*, 1977, **10**, 2239-2251.
20. Y. P. Chong, S. S. Yu, T. J. Fessenden, J. A. Masamitsu, A. M. Frank and D. S. Prono, *J. Appl. Phys.*, 1984, **55**, 611-617.
21. G. Davidson and R. O'Neil, *J. Chem. Phys.*, 1964, **41**, 3946-3955.
22. J. W. Coburn and M. Chen, *J. Appl. Phys.*, 1980, **51**, 3134-3136.
23. E. A. H. Timmermans, J. Jonkers, I. A. J. Thomas, A. Rodero, M. C. Quintero, A. Sola, A. Gamero and J. A. M. v. d. Mullen, *Spectochimica Acta Part B*, 1998, 1553-1566.
24. E. J. Collart, J. A. G. Baggerman and R. J. Visser, *J. Appl. Phys.*, 1991, **70**, 5278-5281.
25. R. E. Walkup, K. L. Saeger and G. S. Selwyn, *J. Chem. Phys.*, 1986, **84**, 2668-2674.
26. M. Touzeau, G. Gousset, J. Jolly, D. Pagnon, M. Vialle, C. M. Ferreira, J. Loureiro, M. Pinheiro and P. A. Sa, in *Nonequilibrium processes in partially ionized gases*, eds. M. Capitelli and J. N. Bardsley, Plenum Press, New York, 1990.
27. A. W. Ali, *The fundamentals of the 3914 A and 3371 A emissions for N_2 and air plasma diagnostics*, NRL-MR-4927, 1982.
28. S. P. Slinker, A. W. Ali and R. D. Taylor, *Production rates for electron beams and swarms in nitrogen*, NRL-MR-6610, 1990.
29. J. D. Jackson, *Classical Electrodynamics*, John Wiley & Sons, Inc., 1967.
30. A. Fridman and L. A. Kennedy, *Plasma physics and engineering*, Taylor & Francis, New York, 2004.
31. A. W. Ali, *Excitation and ionization cross sections for electron beam and microwave energy deposition in air*, NRL-MR-4598, 1981.
32. R. D. Taylor and A. W. Ali, *Excitation and ionization cross sections for electron-beam energy deposition in high temperature air*, NRL-MR-6013, 1987.
33. Hayashi M 2003 *Bibliography of electron and photon cross sections with atoms and molecules published in the 20th centuries: argon* NIFS-DATA-72, National Institute for Fusion Science (Jpn), ISSN 0915-6364.
34. C. Yamabe, S. J. Buckman and A. V. Phelps, *Phys. Rev. A*, 1983, **27**, 1345-1352.
35. J. B. Boffard, B. Chiaro, T. Weber and C. C. Lin, *Atomic Data Nuclear Data Tables*, 2007, **93**, 831-863.
36. V. Konovalov, *Technic. Phys.*, 1993, **63**, 23.
37. L. Christophorou, *Atomic and Molecular Radiation Physics*, Wiley, New York, 1971.
38. D. Leonhardt, C. Muratore and S. G. Walton, *IEEE Trans. Plasma Sci.*, 2005, **33**, 783-790.
39. G. Davidson and R. O'Neil, *J. Chem. Phys.*, 1964, **41**, 3946-3956.
40. Mitchell, *J. Chem. Phys.*, 1970, **53**, 1795.
41. Hirsch, *Phys. Rev. A*, 1970, **1**, 1615.
42. F. Zhe, G. Zhigang, P. Yukang and Z. Xiaozhang, *Plasma Sci. Technology*, 2010, **12**, 304-309.
43. X. Zhu and Y. Pu, *J. Phys. D: Appl. Phys*, 2010, **43**, 015204.
44. T. Czerwiec, F. Greer and D. B. Graves, *J. Phys. D: Appl. Phys.*, 2005, **38**, 4278-4289.
45. A. Qayyum, S. Zeb, S. Ali, A. Waheed and M. Zakaullah, *Plasma Chem. Plasma Process.*, 2005, **25**, 551-564.
46. C. M. Ferreira and J. Loureiro, *J. Phys. D: Appl. Phys.*, 1984, **17**, 1175-1188.
47. E. H. Lock, S. G. Walton and R. F. Fernsler, *Plasma Process. Polymers*, 2009, **6**, 234-245.
48. S. P. Slinker, A. W. Ali and R. D. Taylor, *J. Appl. Phys.*, 1990, **67**, 679-690.

10. Appendix

a) *Optical emission spectra*

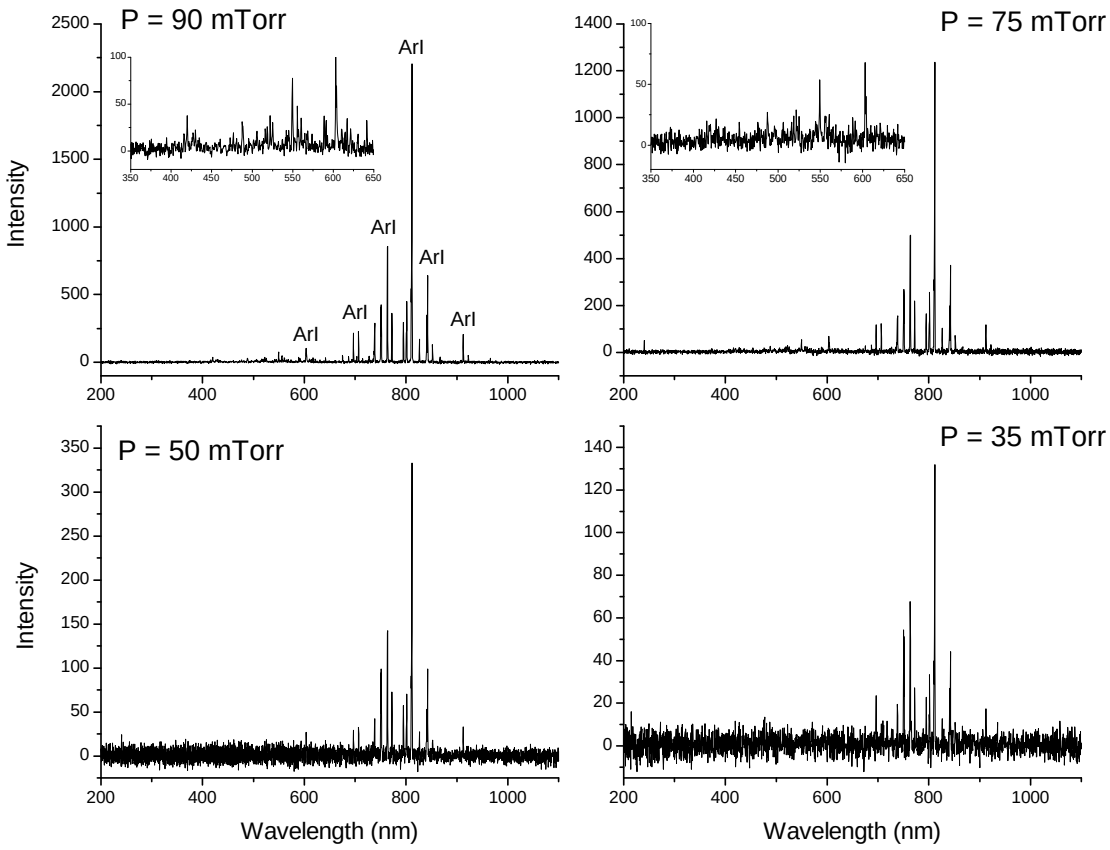

Figure 8-1. OES spectra in pulsed electron beam-generated plasma in argon as a function of pressure (10 % duty)

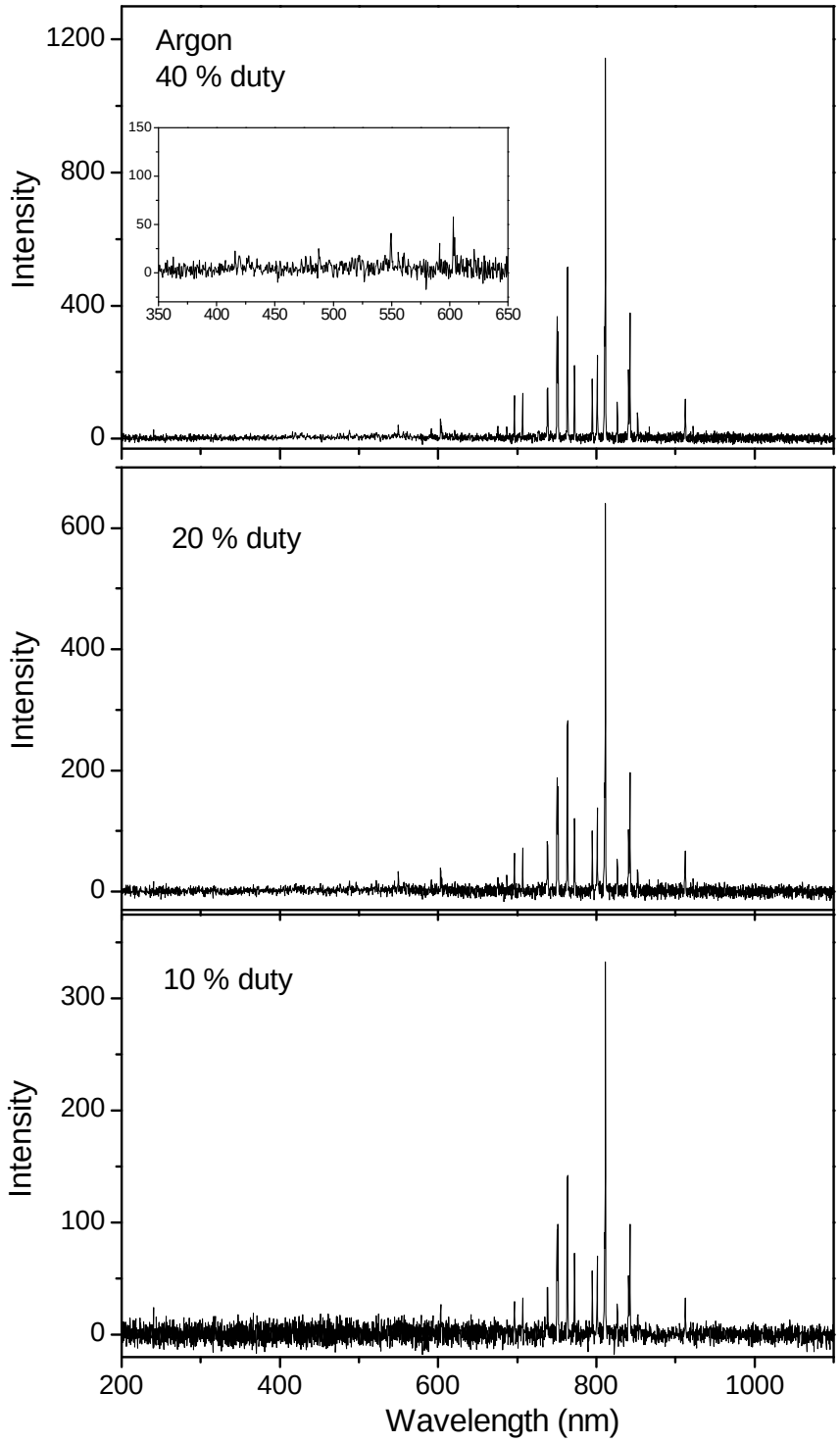

Figure 8-2. OES spectra in pulsed electron beam-generated plasma in argon as a function of duty (p = 50 mTorr)

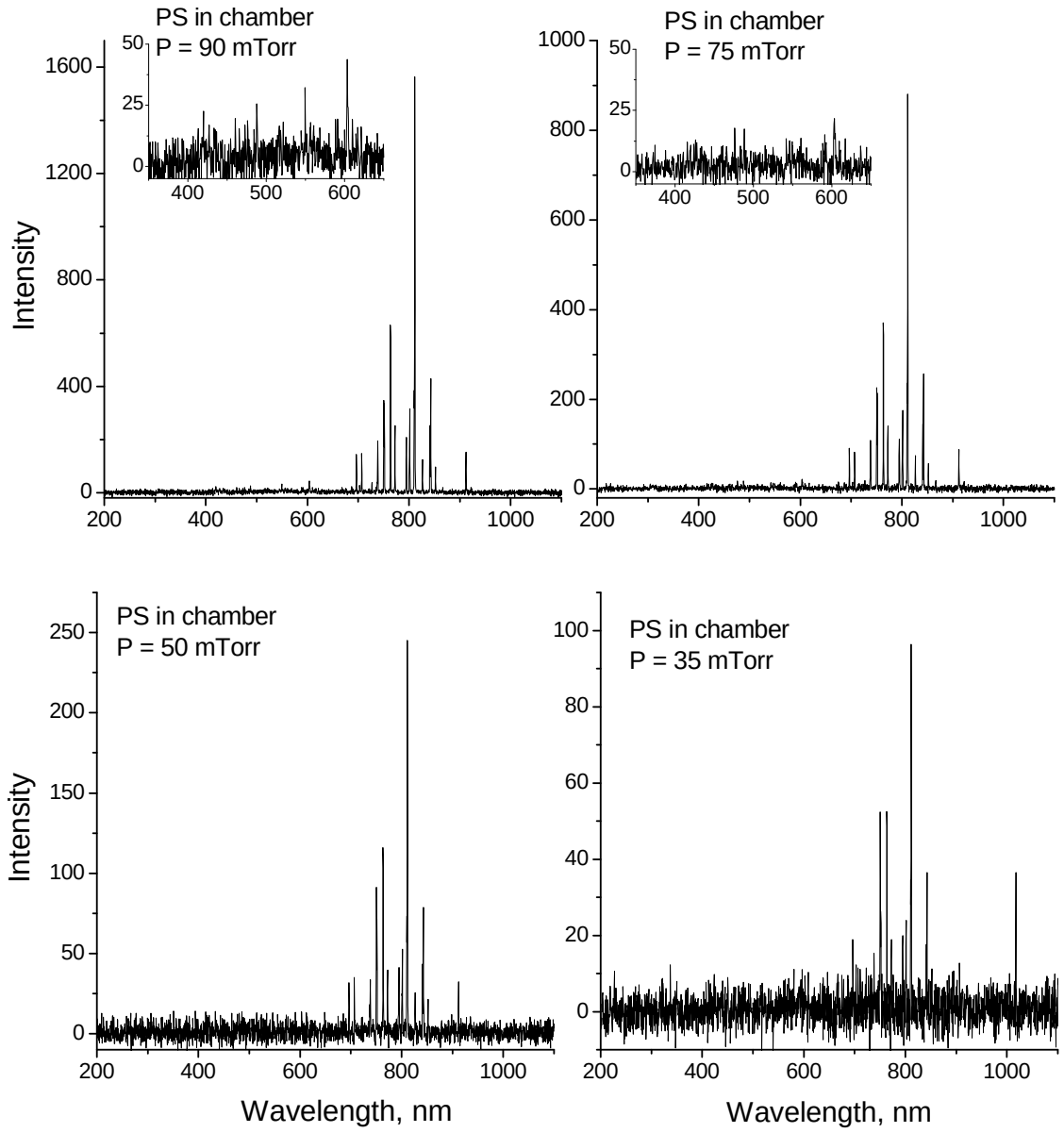

Figure 8-3. OES spectra in pulsed electron beam-generated plasma in argon as a function of pressure when polystyrene is present in the chamber (10 % duty factor). It should be noted that the overall emission intensity is reduced and the intensity of the singly charged excited argon ions are reduced to noise levels.

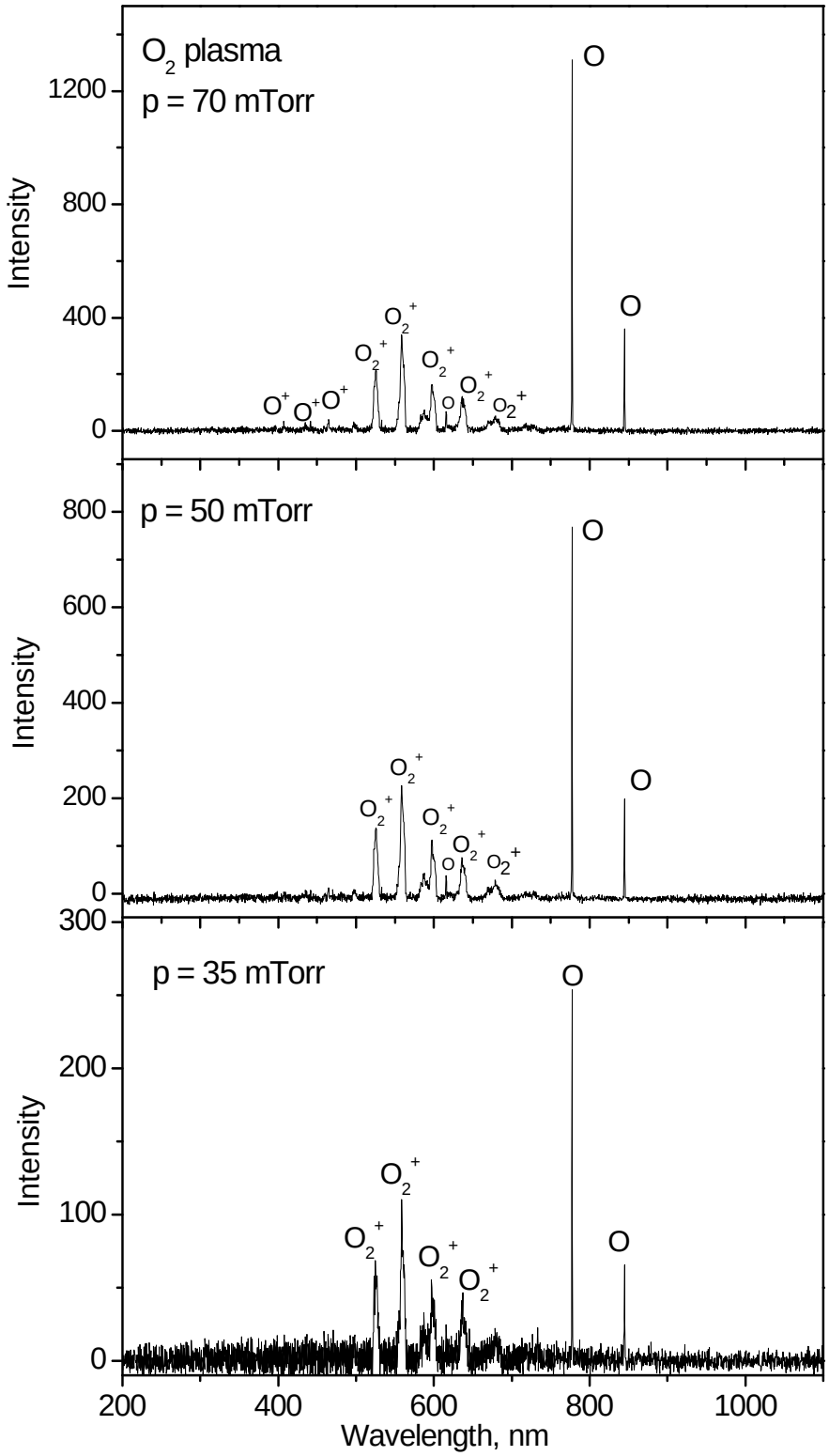

Figure 8-4. OES spectra in pulsed electron beam-generated plasma in oxygen as a function of pressure.

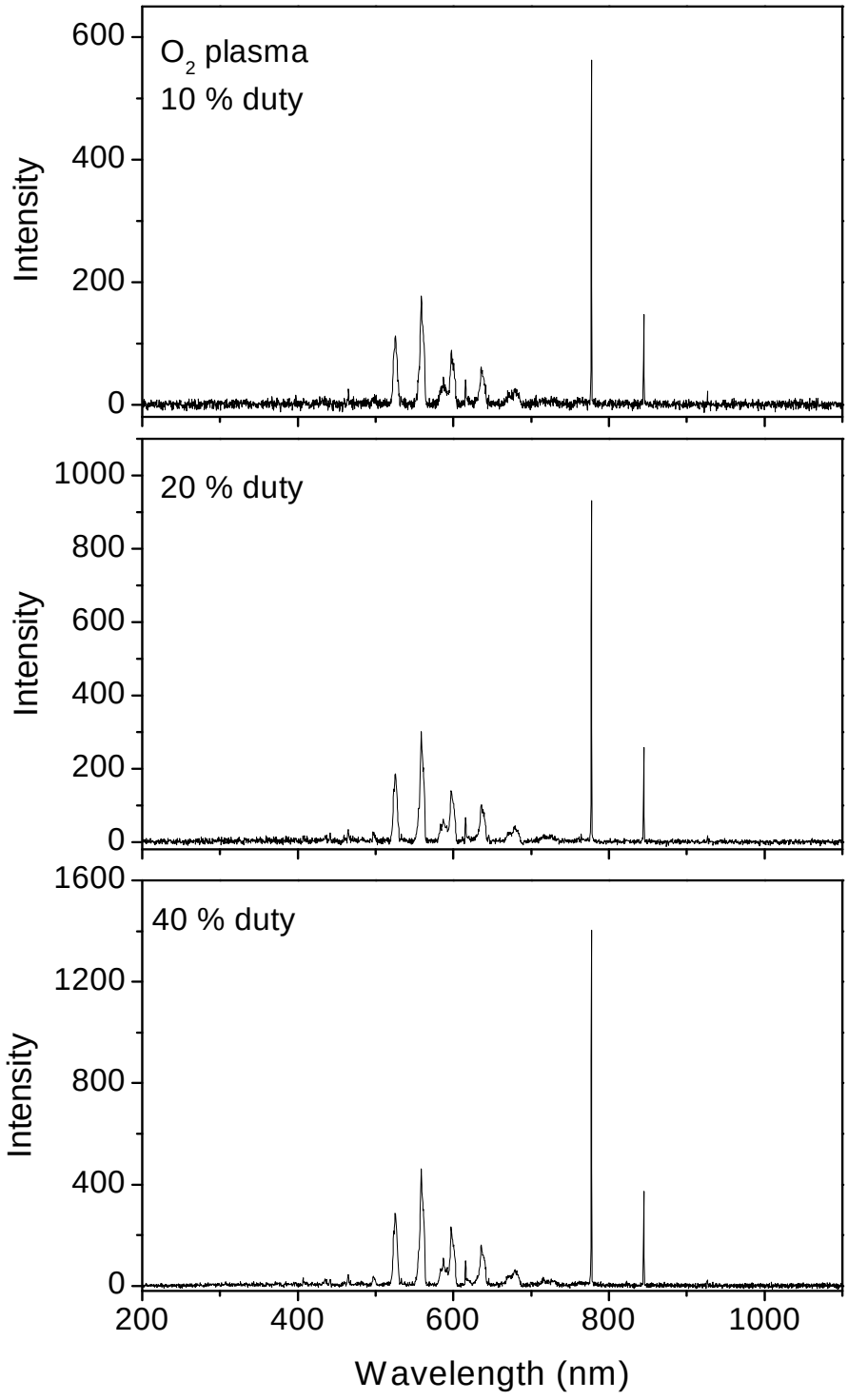

Figure 8-5. OES spectra in pulsed electron beam-generated plasma in oxygen as a function of duty factor.

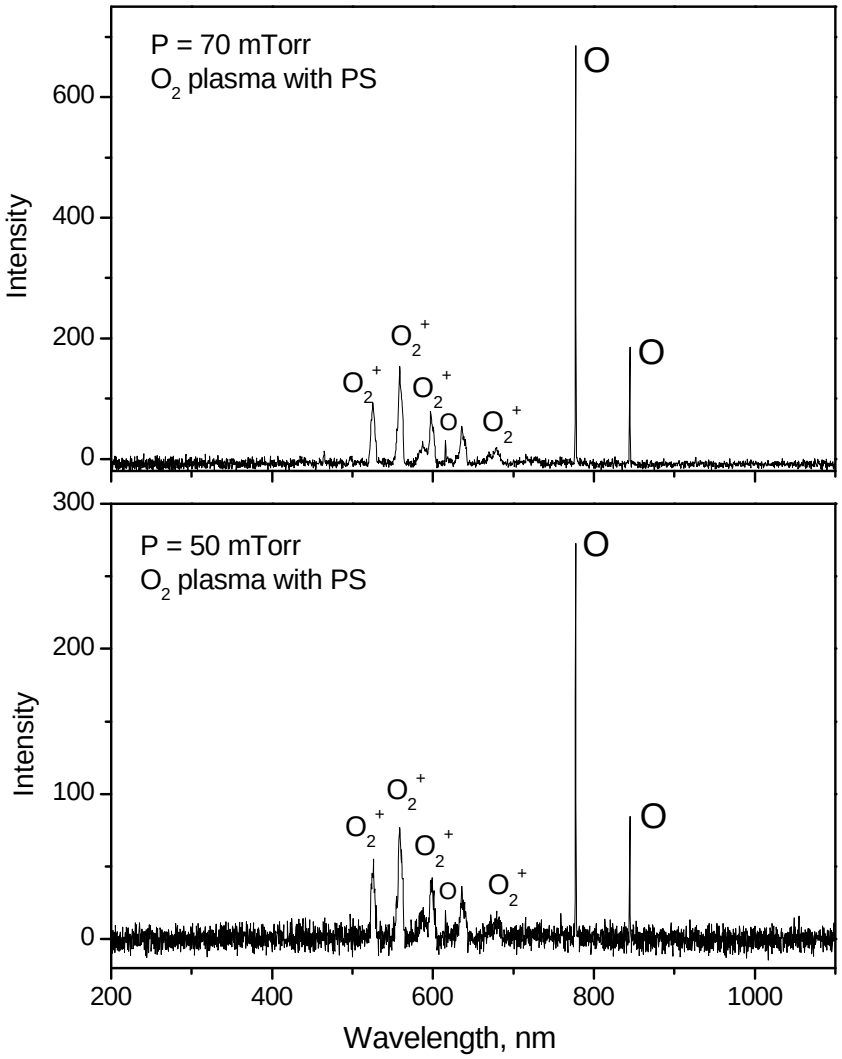

Figure 8-6. OES spectra in pulsed electron beam-generated plasma in oxygen with polystyrene present in the chamber (duty factor 10 %).

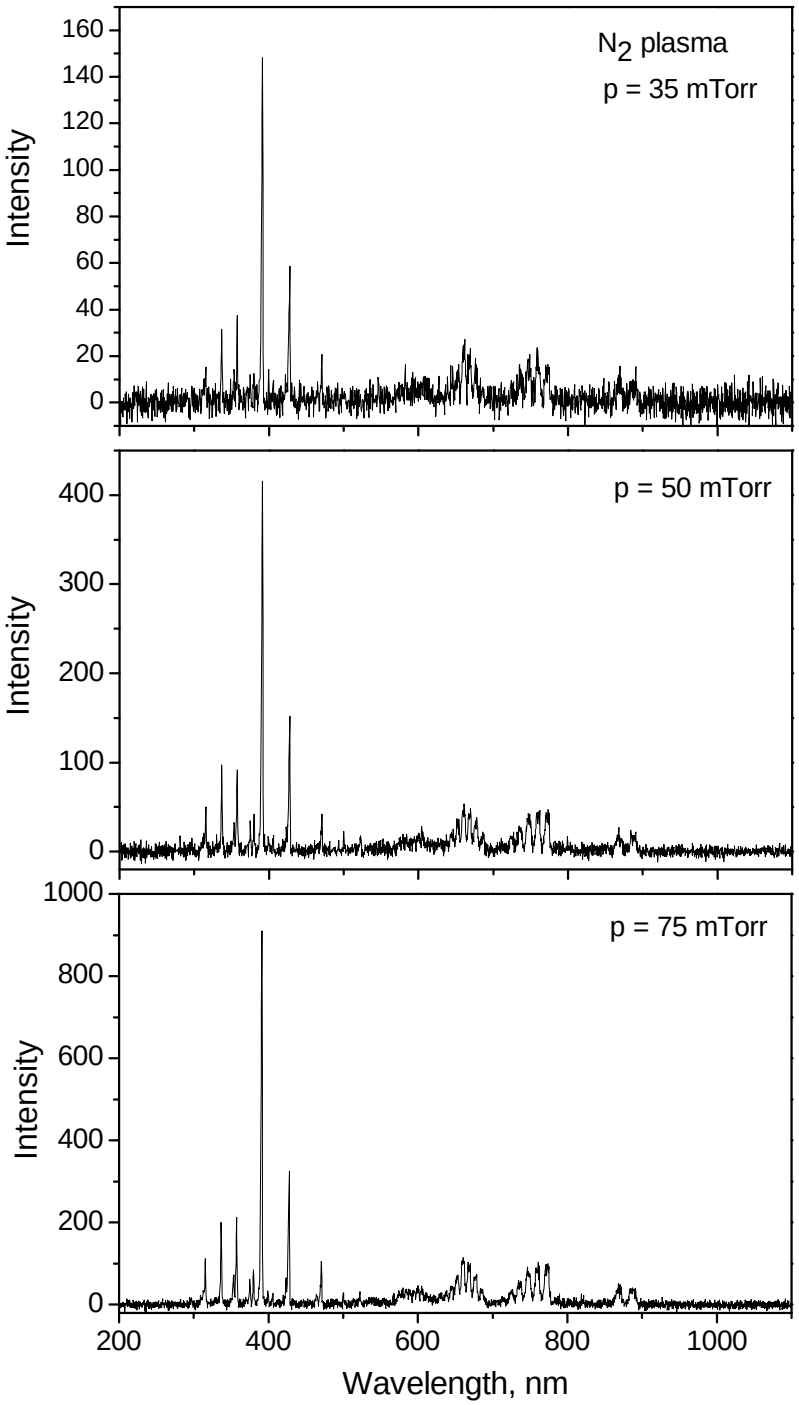

Figure 8-7. OES spectra in pulsed electron beam-generated plasma in nitrogen as a function of pressure.

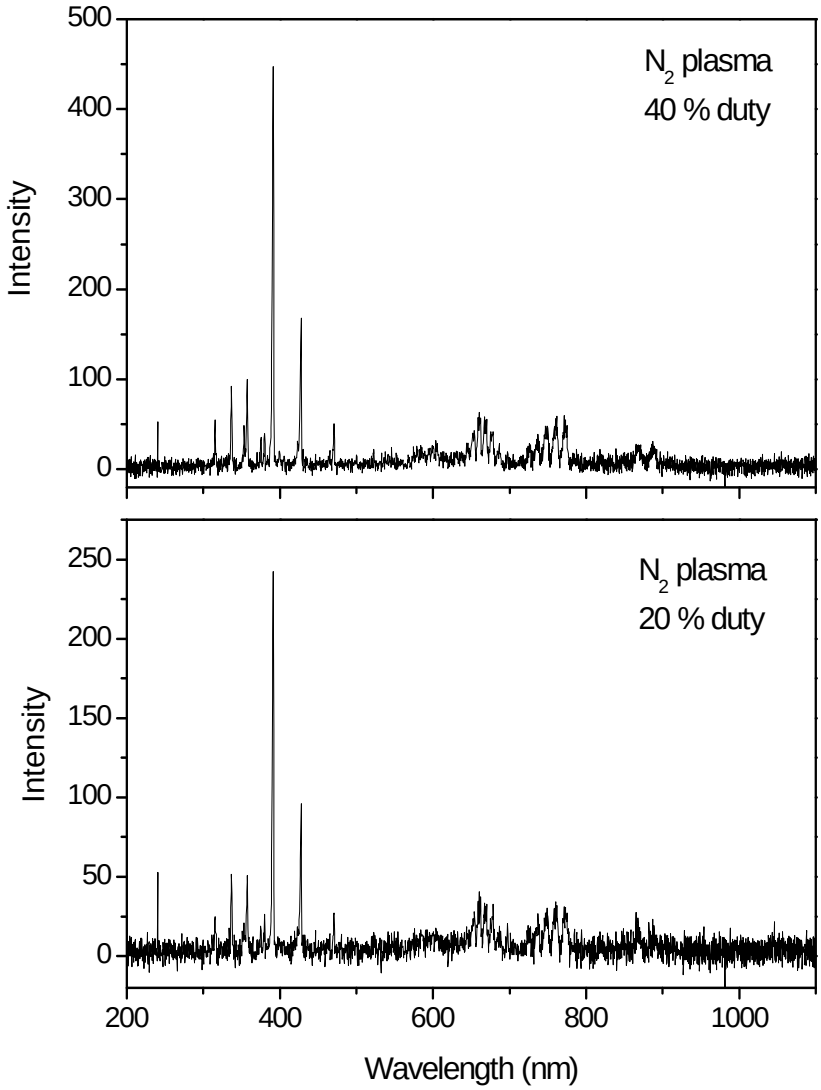

Figure 8-8. OES spectra in pulsed electron beam-generated plasma in nitrogen as a function of duty factor.

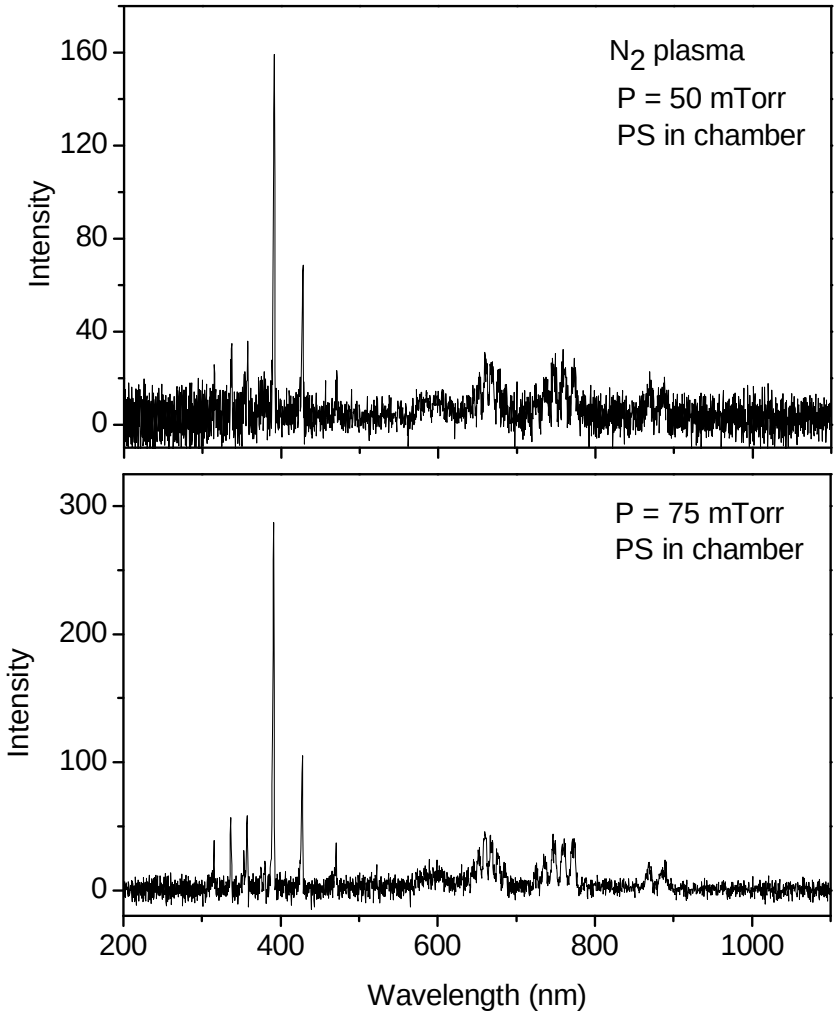

Figure 8-9. OES spectra in pulsed electron beam-generated plasma in nitrogen with polystyrene present in the chamber.

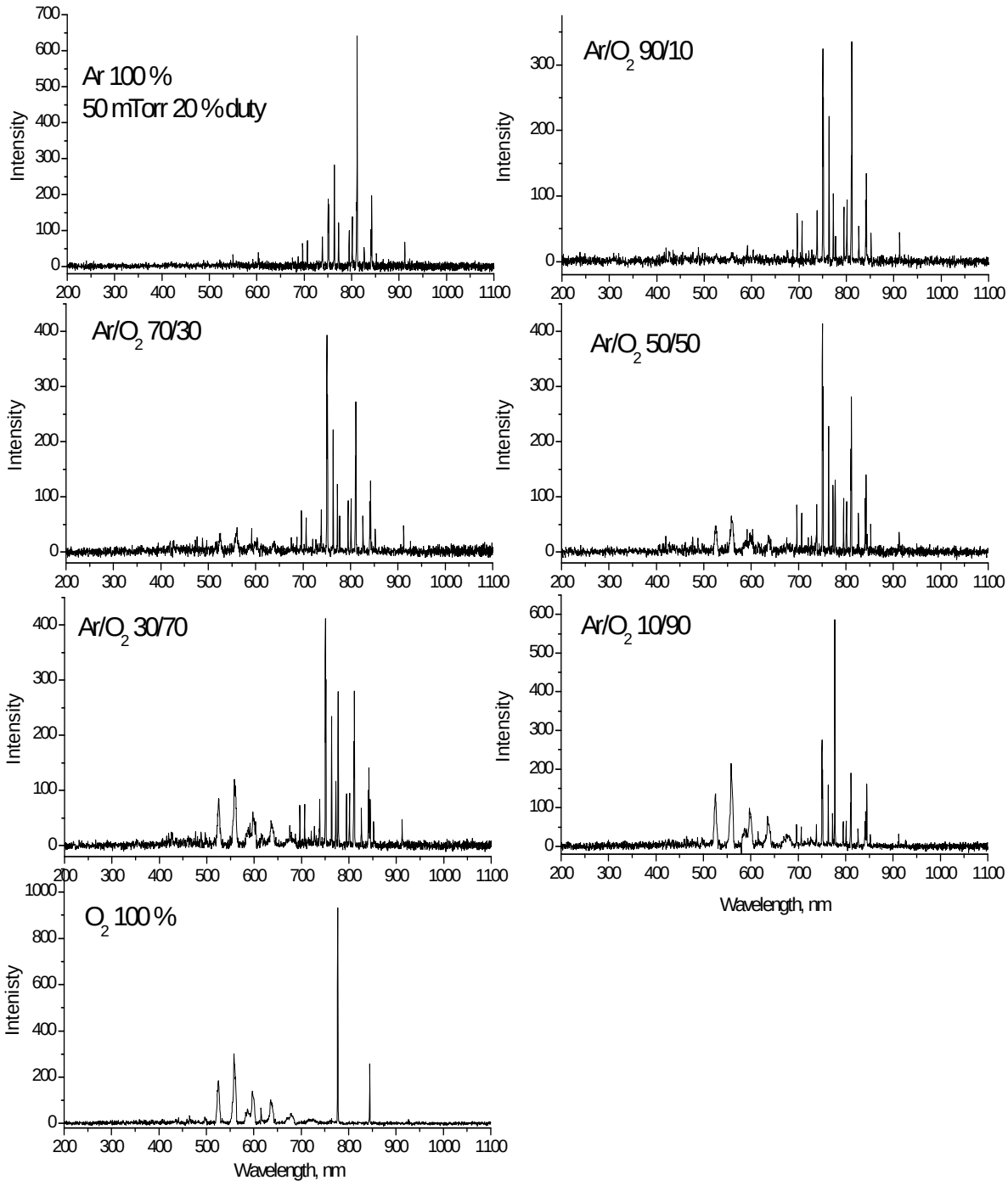

Figure 8-10. OES spectra in pulsed electron beam-generated plasma in Ar/O_2 mixtures at p = 50 mTorr and 20 % duty factor.

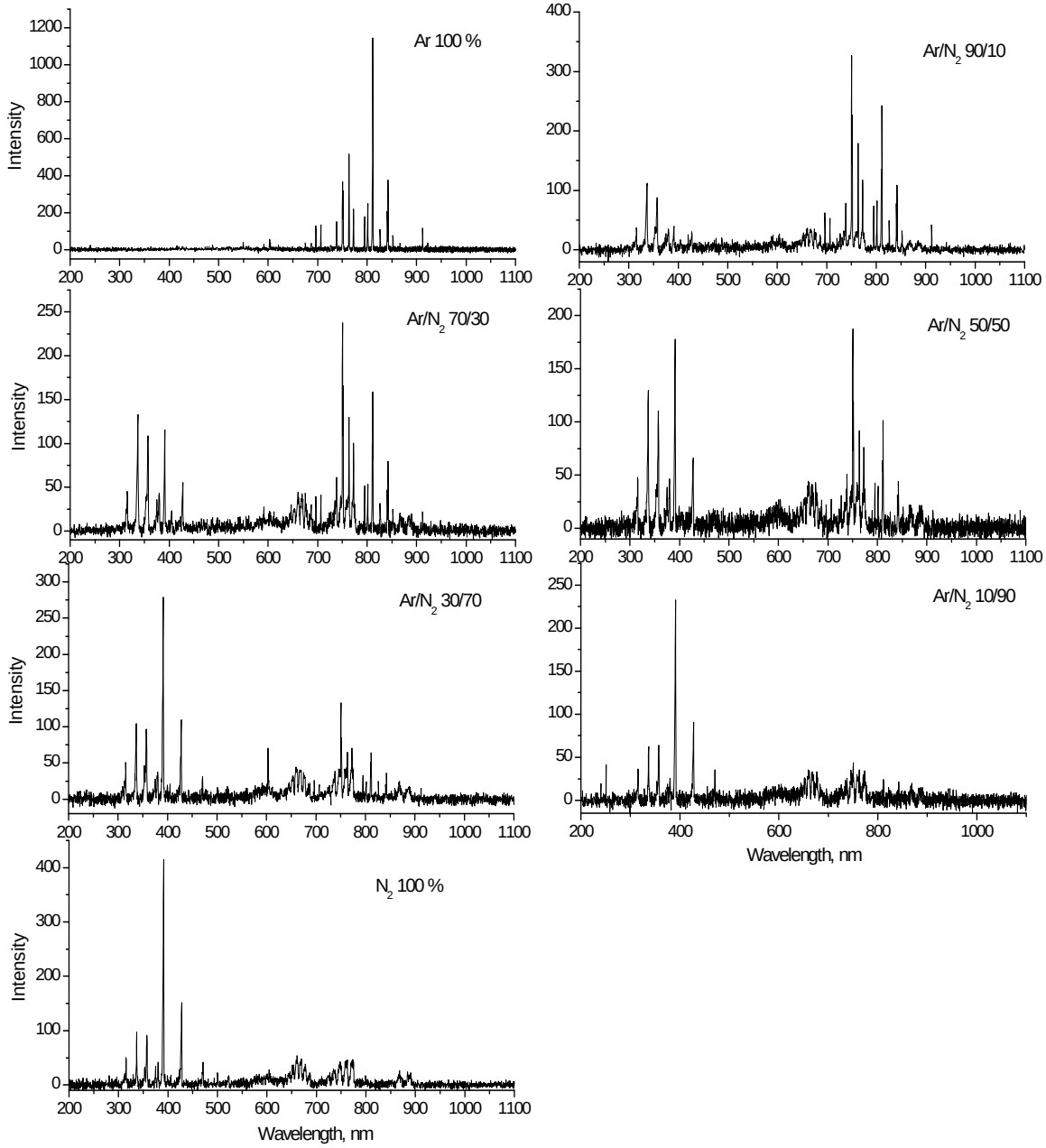

Figure 8-11. OES spectra in pulsed electron beam-generated plasma in Ar/N_2 mixtures at p = 50 mTorr and 40 % duty factor.

b) ***Used cross sections for argon, nitrogen and oxygen in PLUME***

i. Argon

The plotted cross sections for argon are from Bretagne.

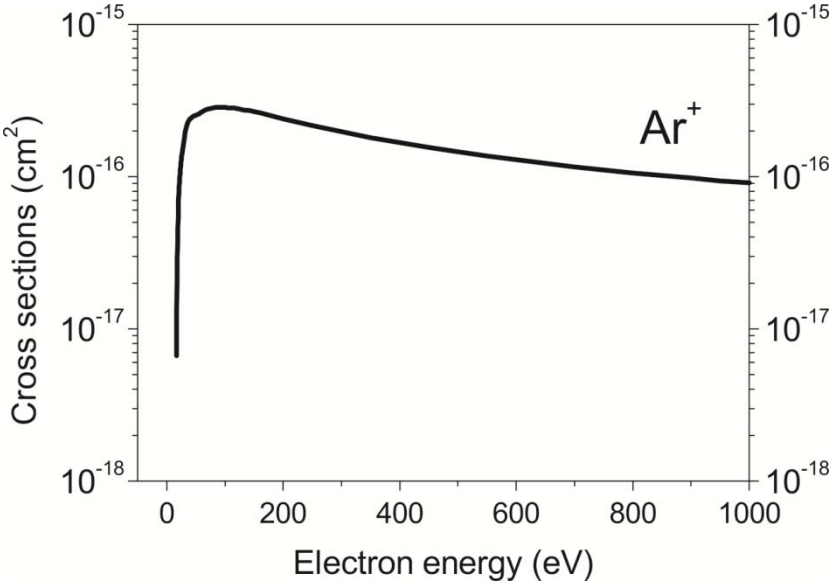

Figure 8-12. Ionization cross section

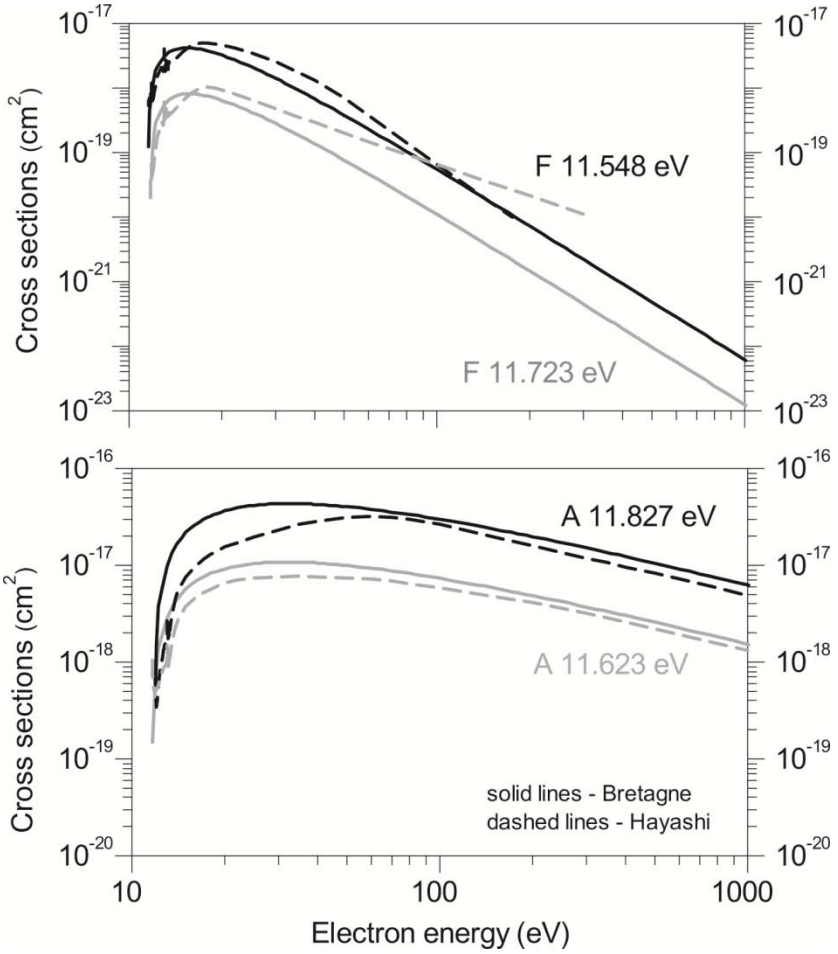

Figure 8-13. Major allowed (A) and forbidden (F) states in argon.

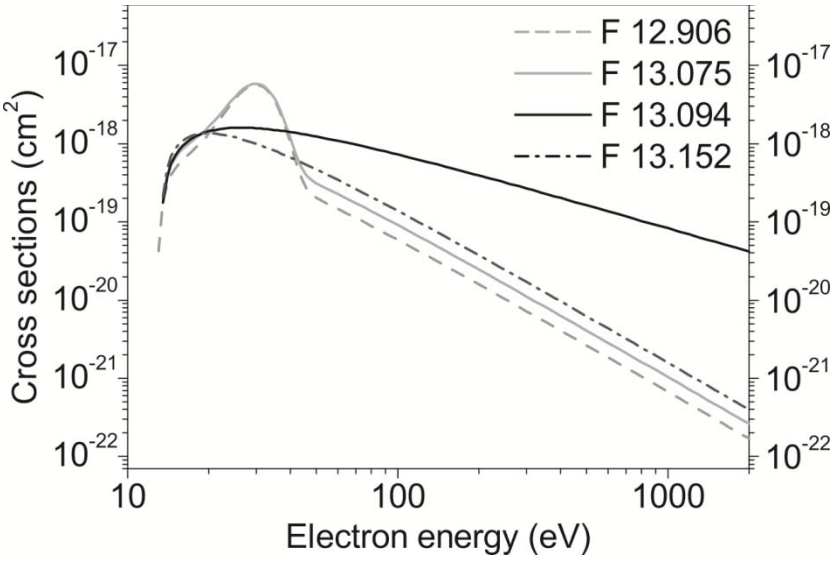

Figure 8-14. Forbidden (F) states in argon. Energy levels 12.906-13.152 eV.

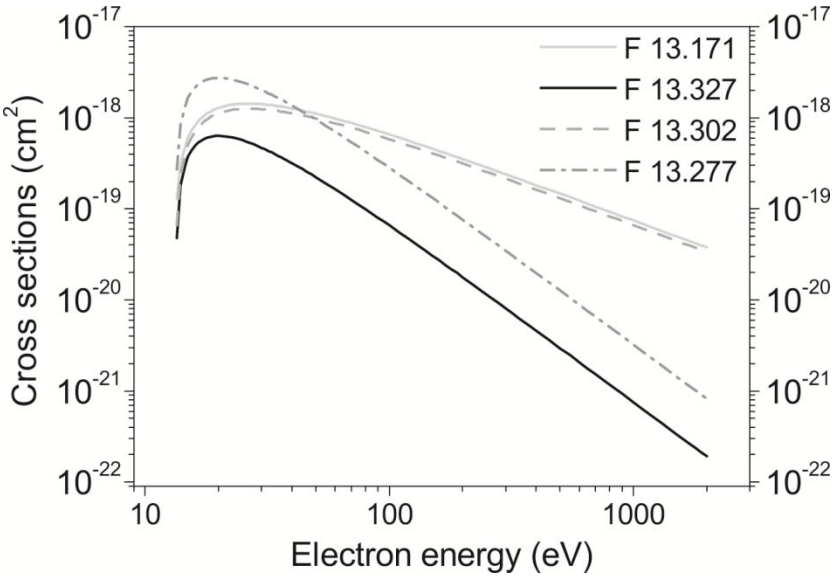

Figure 8-15. Forbidden (F) states in argon. Energy levels 13.171-13.277 eV.

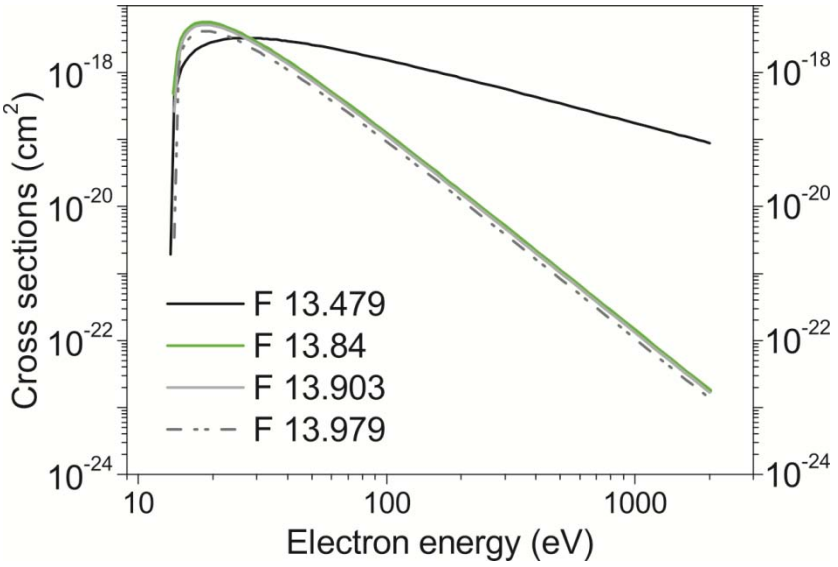

Figure 8-16. Forbidden (F) states in argon. Energy levels 13.479-13.979 eV.

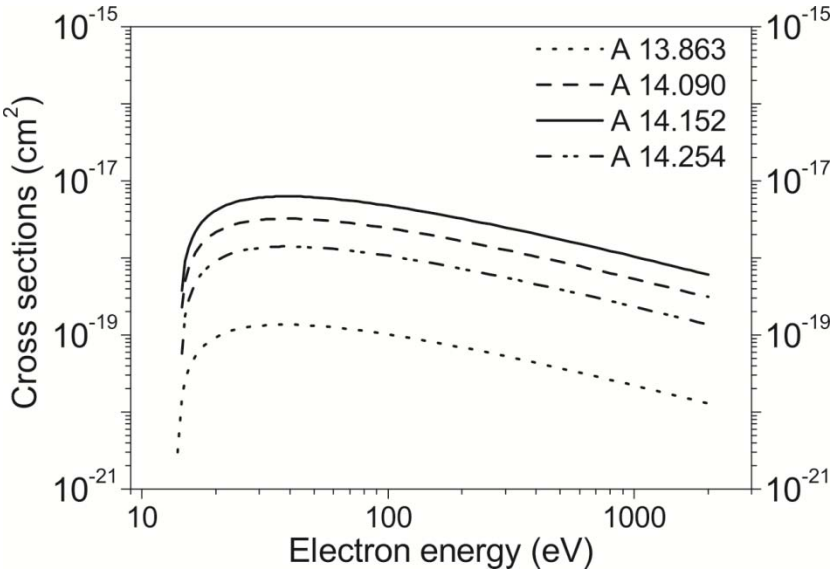

Figure 8-17. Allowed (A) states in argon. Energy levels 13.863-14.303 eV.

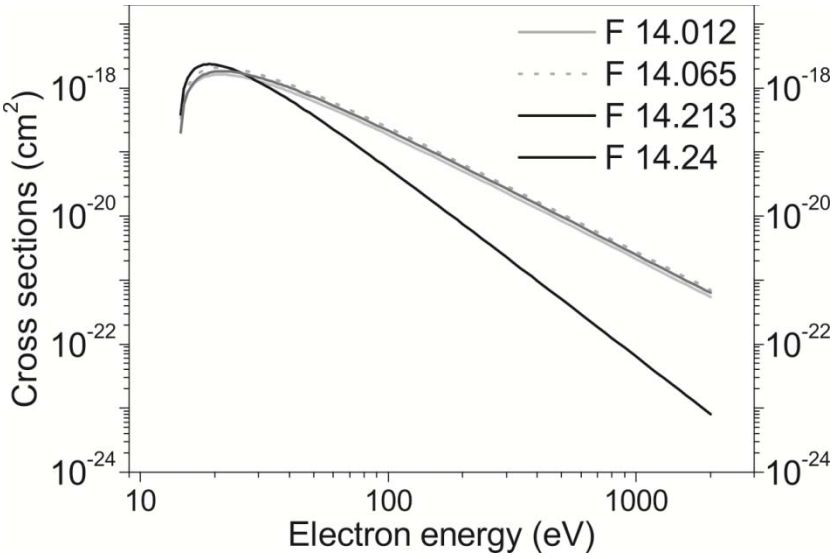

Figure 8-18. Forbidden (F) states in argon. Energy levels 14.012-14.24 eV.

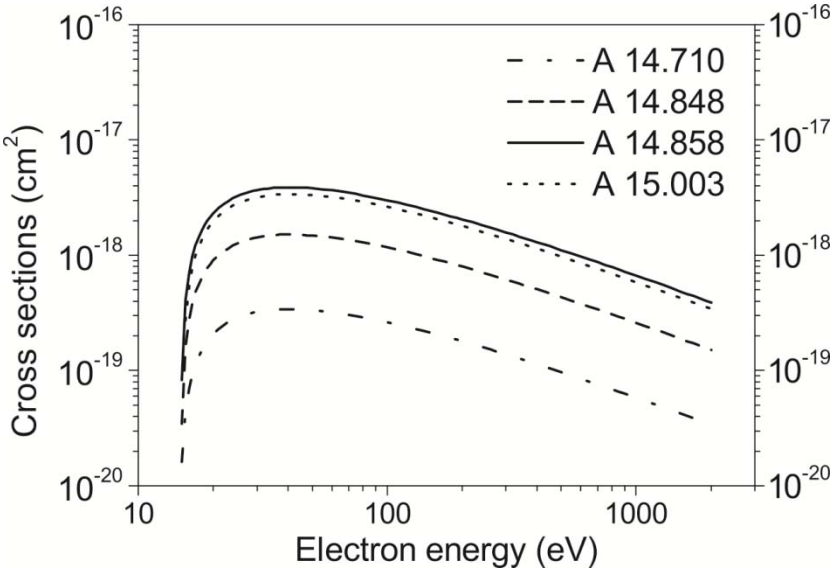

Figure 8-19. Allowed (A) states in argon. Energy levels 14.710-15.003 eV.

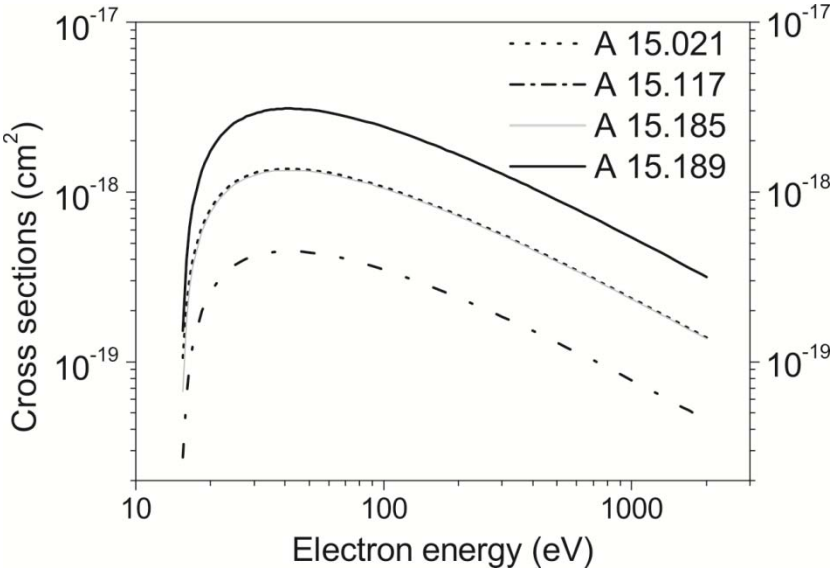

Figure 8-20. Allowed (A) states in argon. Energy levels 15.021-15.189 eV.

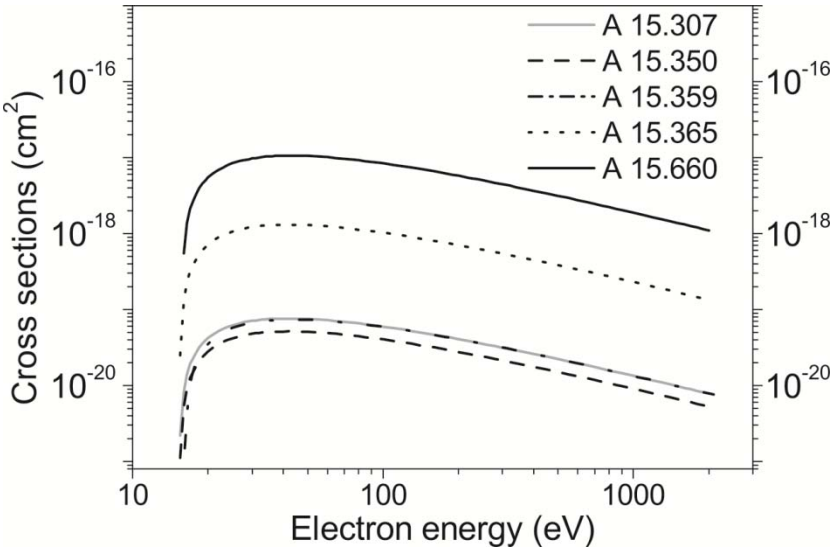

Figure 8-21. Allowed states in argon. Energy levels 15.307-15.660 eV.

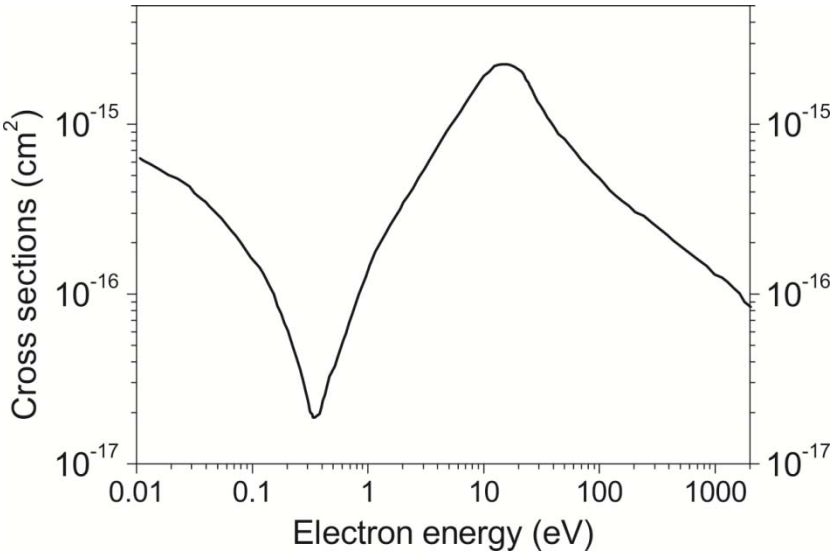

Figure 8-22. Elastic collisions cross section in argon.

ii. Nitrogen

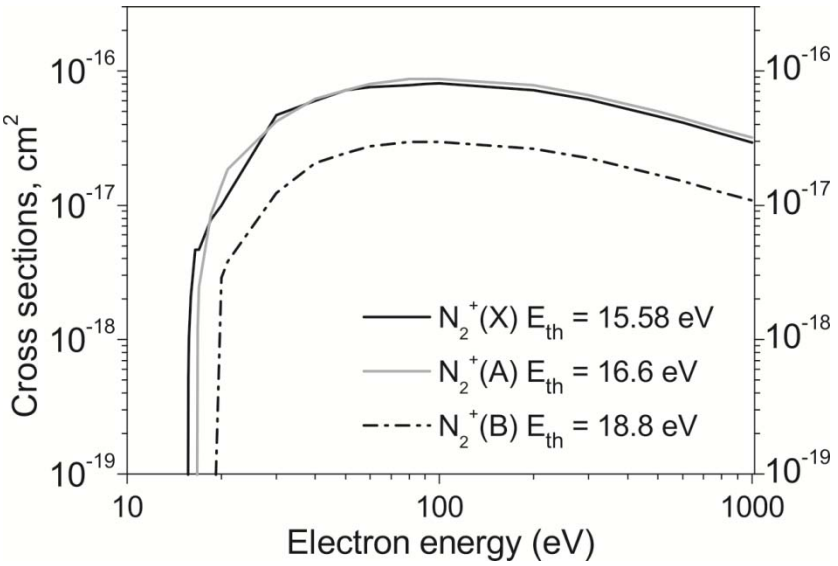

Figure 8-23. Ionization cross sections in nitrogen. E_{th} denotes threshold energy of the state.

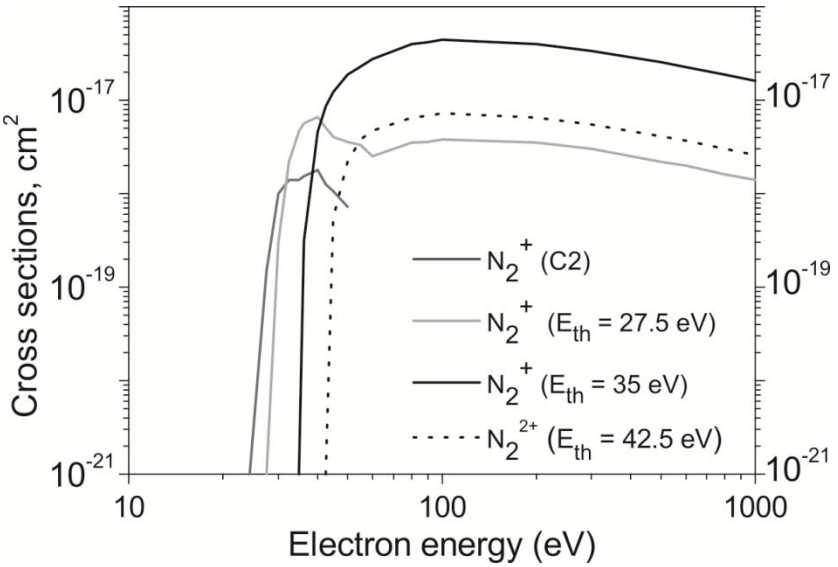

Figure 8-24. Dissociative ionization cross sections in nitrogen.

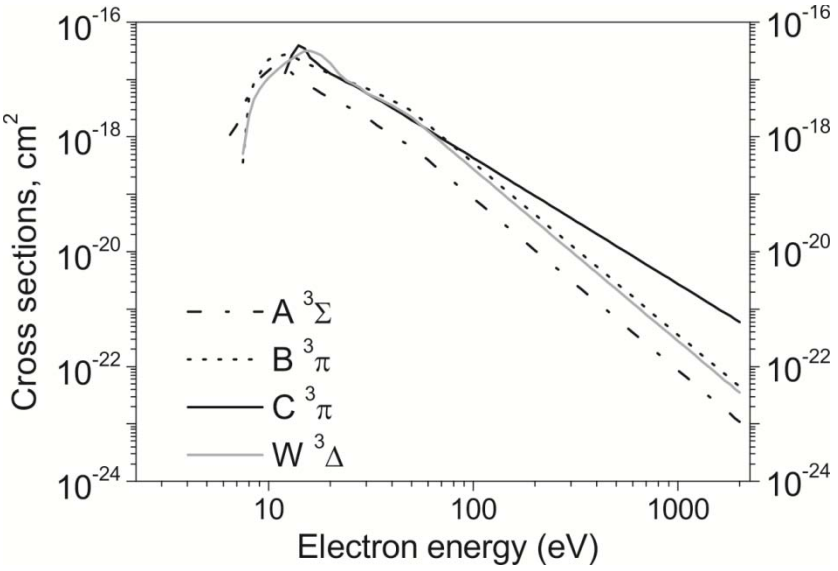

Figure 8-25. Extension for electron impact excitation cross sections for $A^3\Sigma$, $B^3\pi$, $C^3\pi$, $W^3\Delta$ as calculated by PLUME.

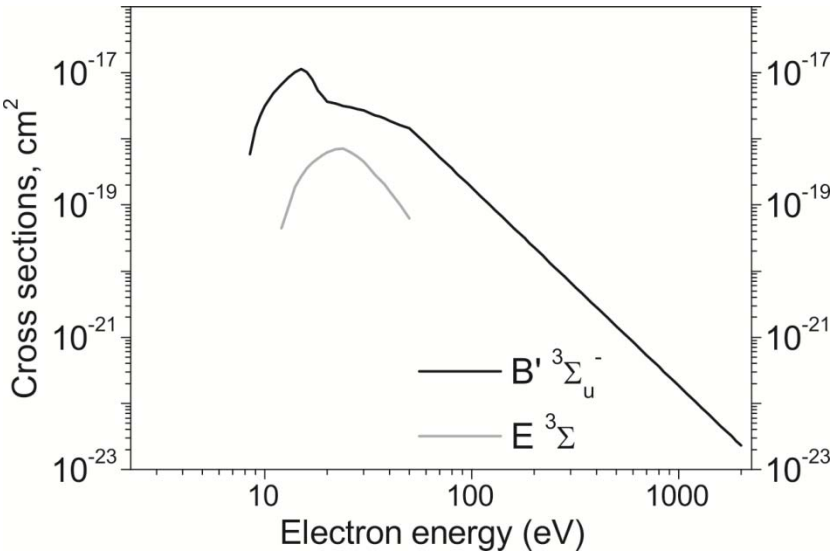

Figure 8-26. Extension for electron impact excitation cross sections for $B'^3\Sigma_u^-$ as calculated by PLUME.

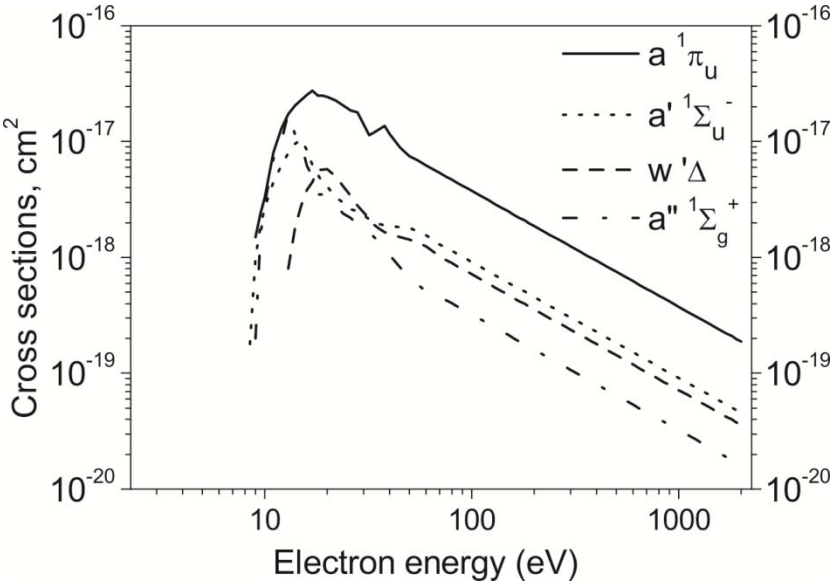

Figure 8-27. Extension for electron impact excitation cross sections for $a^1\pi_u$, $a'^1\Sigma_u^-$, $w'\Delta$ and $a''^1\Sigma_u^+$ as calculated by PLUME.

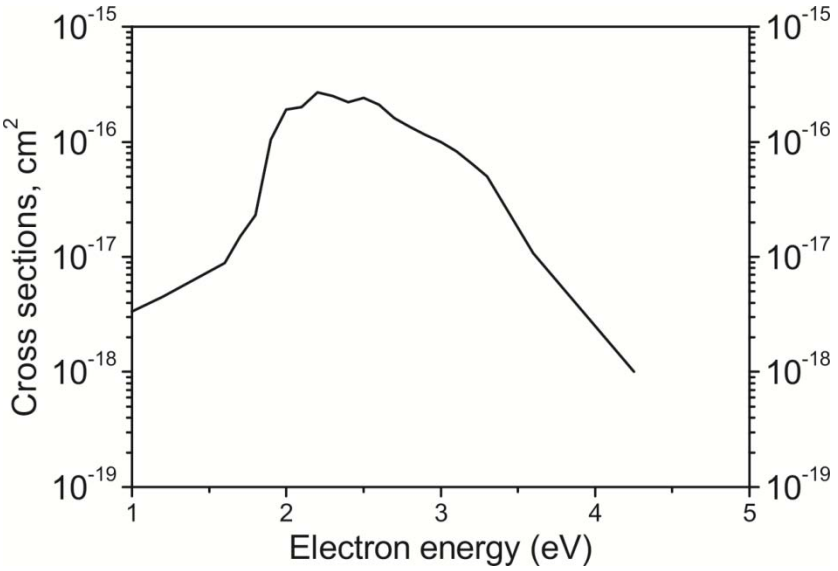

Figure 8-28. Electron impact excitation cross sections of rotational levels.

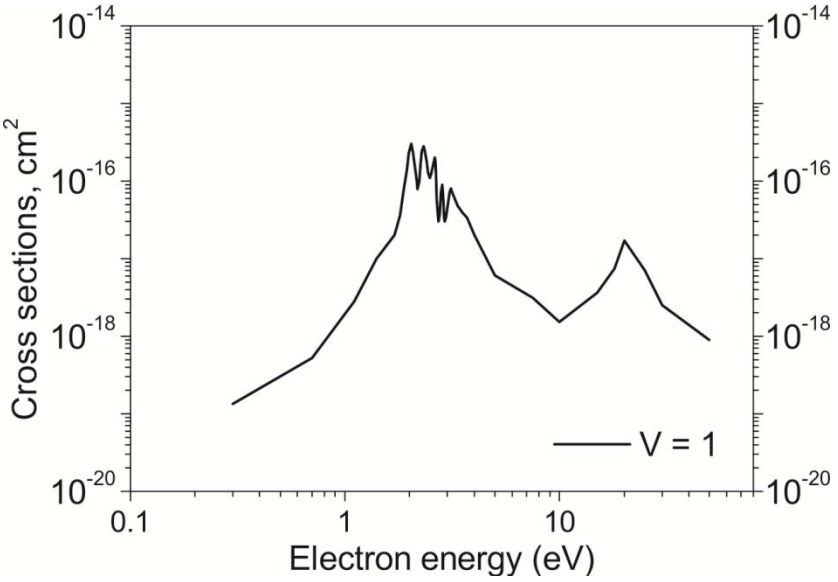

Figure 8-29. Electron impact excitation of the first ground state vibrational level.

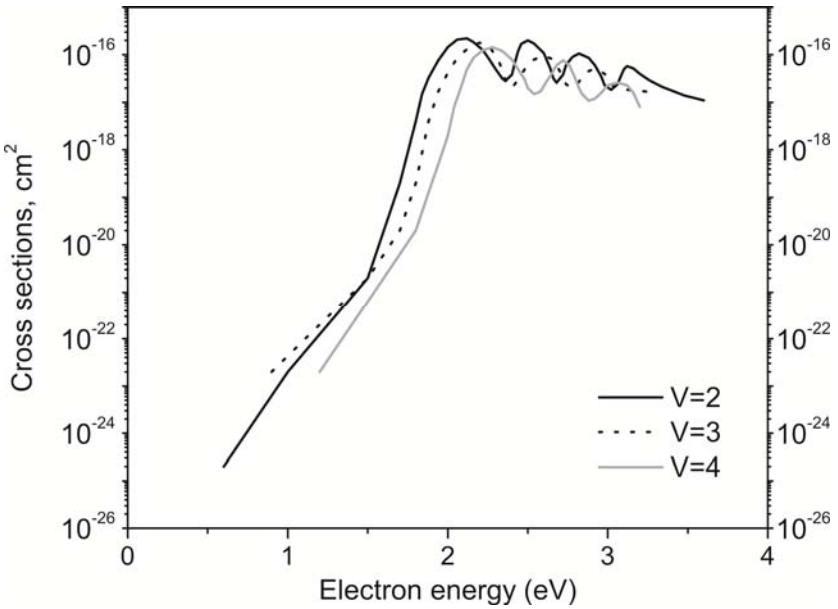

Figure 8-30. Electron impact excitation of the vibrational levels 2 - 4.

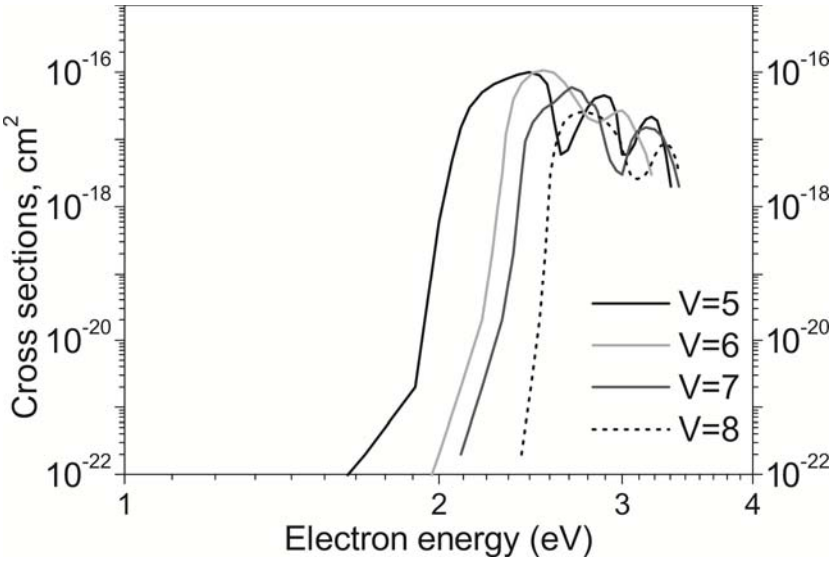

Figure 8-31. Electron impact excitation of the vibrational levels 5 - 8.

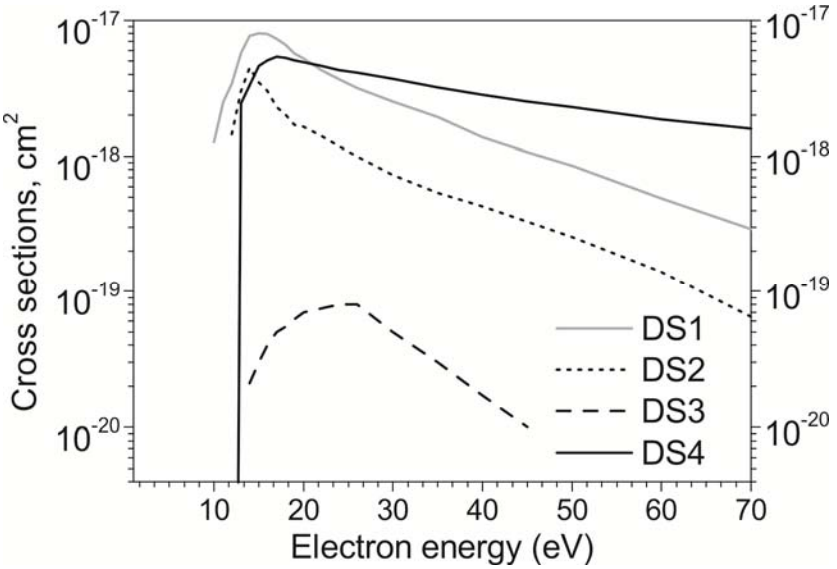

Figure 8-32. Dissociation cross sections. DS 1-DS 3 corresponds to the contribution of the triplet states. DS4 is the contribution of $a^1\Pi$ state, which amounts to the 18 % of the total cross section.

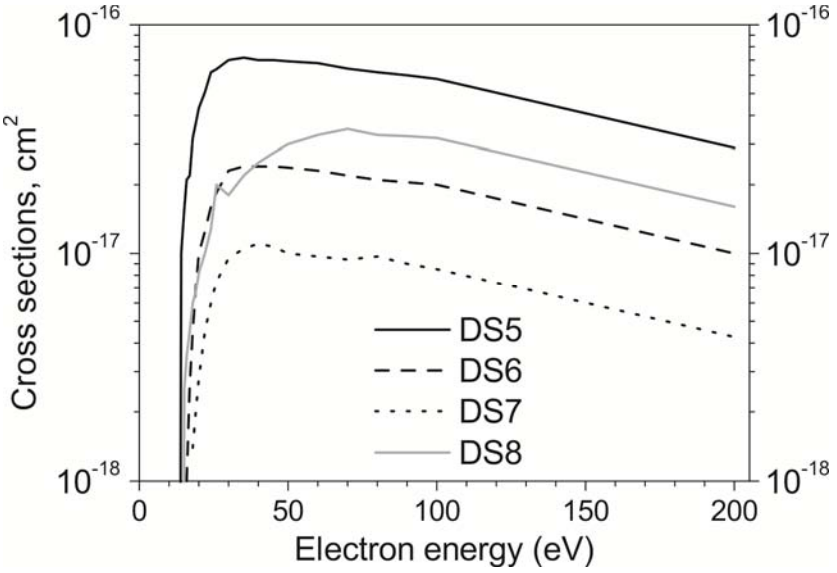

Figure 8-33. Dissociation cross sections. DS 5 corresponds to the contribution of the $b^1\Pi$ family of states. DS 6 is the peak observed at 15.8 eV. DS 7 is associated with a state at 17.3 eV. DS 8 is for $c^1\Sigma$ states.

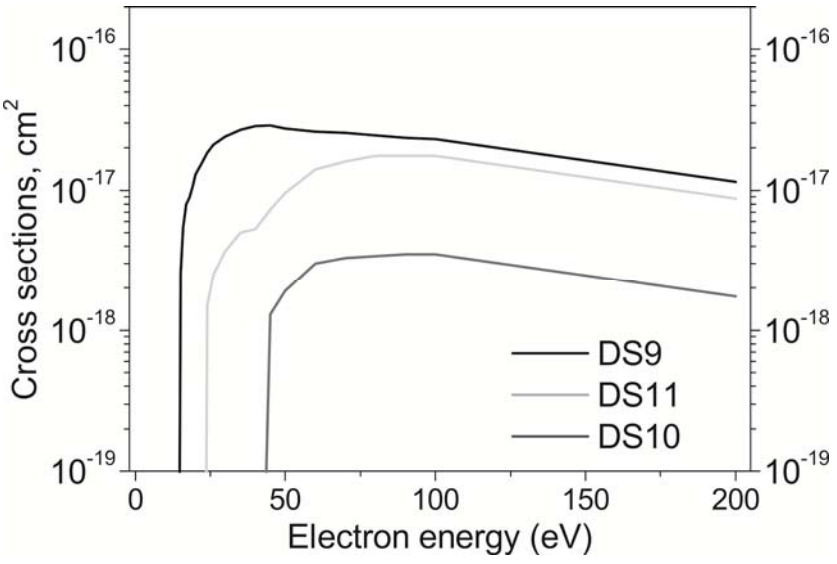

Figure 8-34. Dissociation cross sections. DS 9 corresponds to the $b^1\Sigma_u$ states, DS 10 to the Rydberg states, and DS 11 to the UV emitting states.

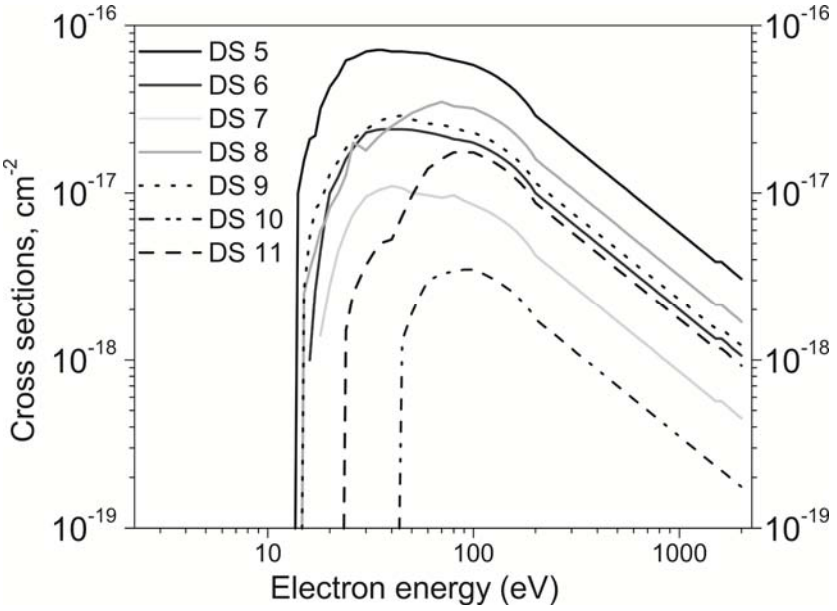

Figure 8-35. Extensions for the dissociation cross sections for DS5 – DS 11 as calculated by PLUME.

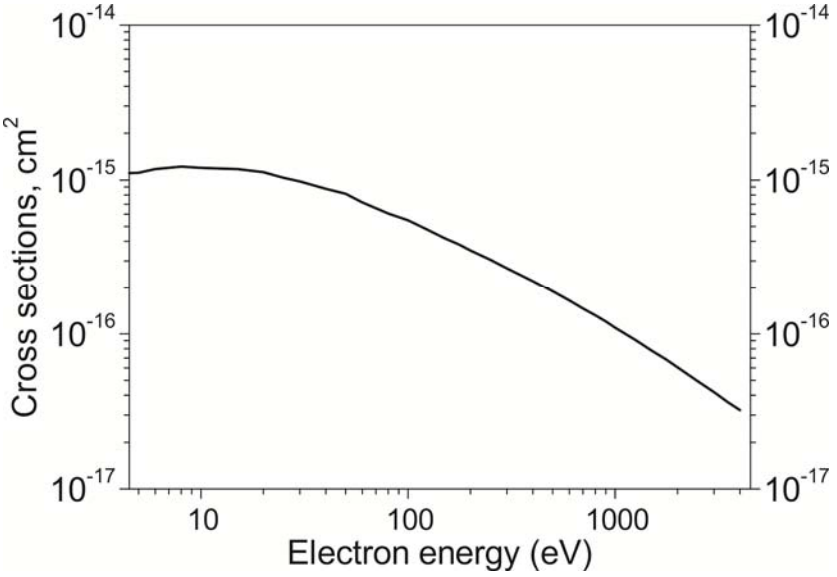

Figure 8-36. Cross sections for elastic collisions.

iii. Oxygen

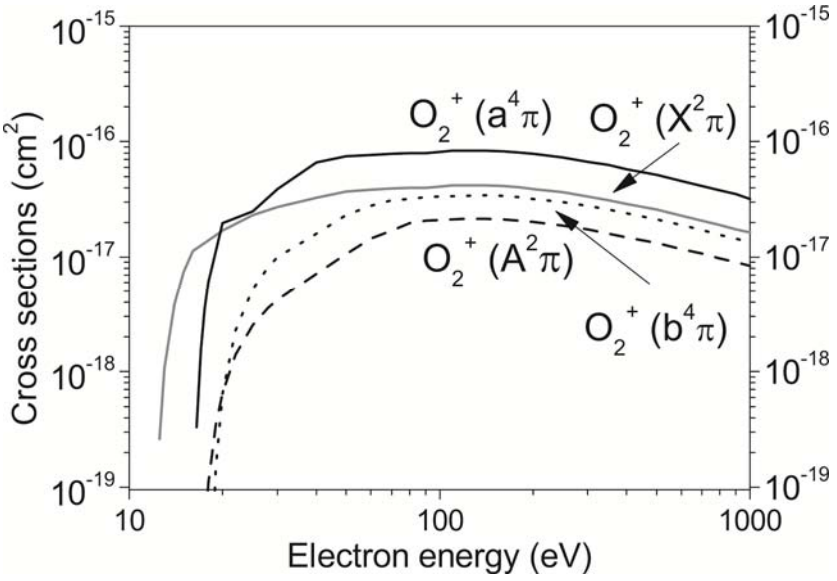

Figure 8-37. Oxygen ionization cross sections. Threshold energies for O_2^+(X), O_2^+(a), O_2^+(A), O_2^+(b) are 12.06 eV, 16.1 eV, 16.9 eV and 18.2 eV respectively.

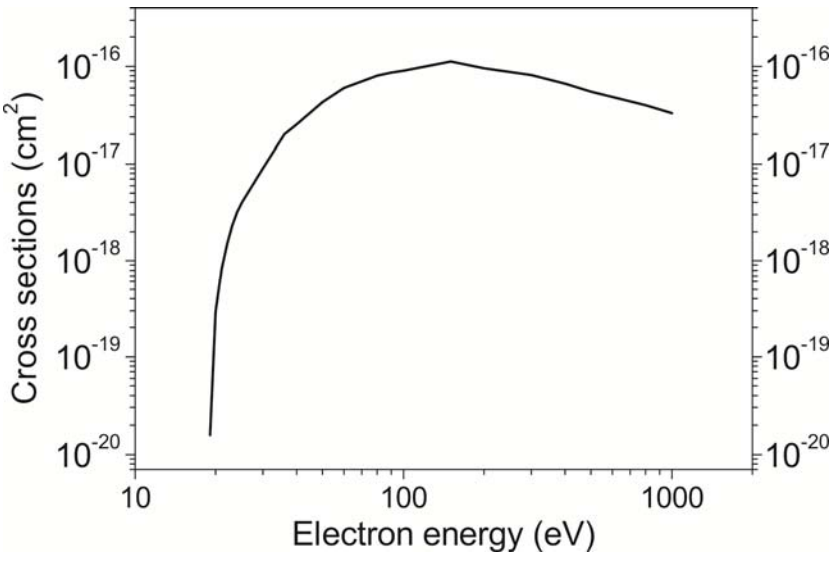

Figure 8-38. Dissociative ionization cross section.

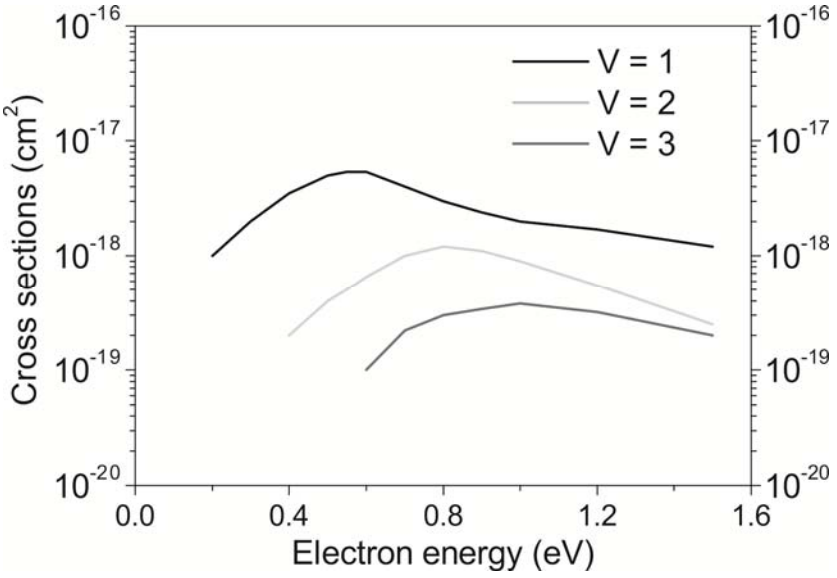

Figure 8-39. Electron impact excitation cross sections for ground state vibrational levels of O_2.

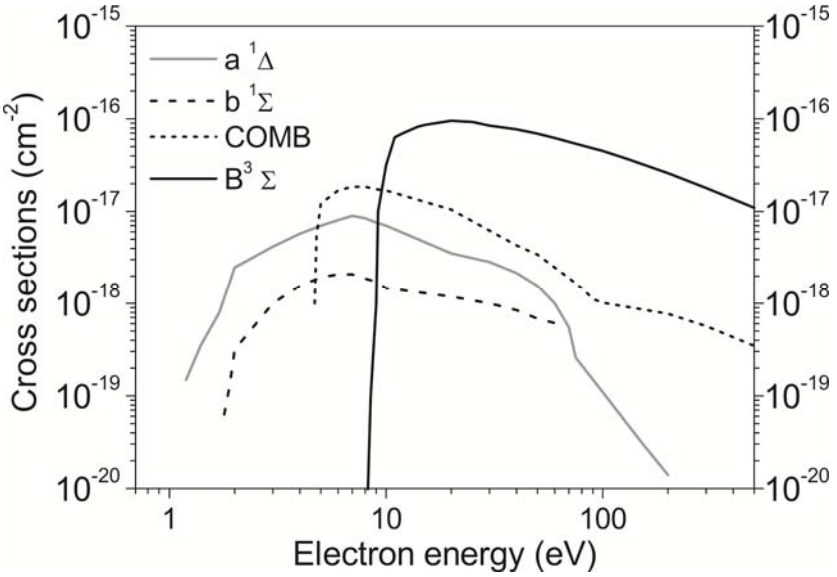

Figure 8-40. Cross section for electron impact excitation of oxygen. COMB denotes $A^3\Sigma+C^3\Delta+C^1\Sigma$.

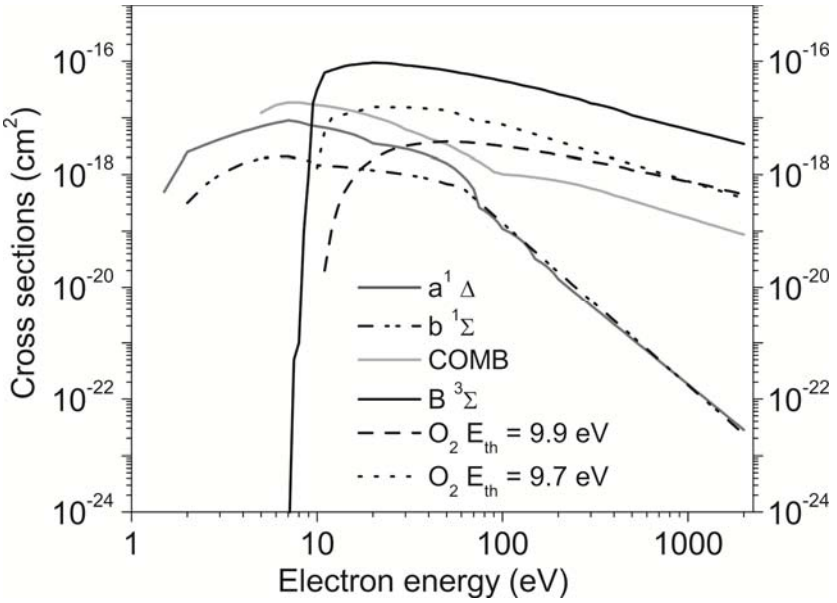

Figure 8-41. Cross section for electron impact excitation of oxygen as calculated by PLUME. COMB denotes $A^3\Sigma+C^3\Delta+C^1\Sigma$.

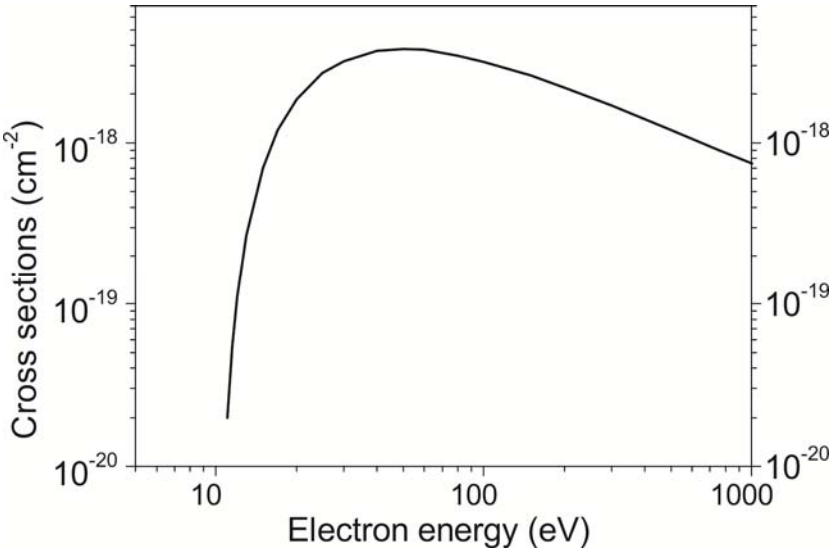

Figure 8-42. Extensions for Rydberg state cross section for electron impact excitation of oxygen.

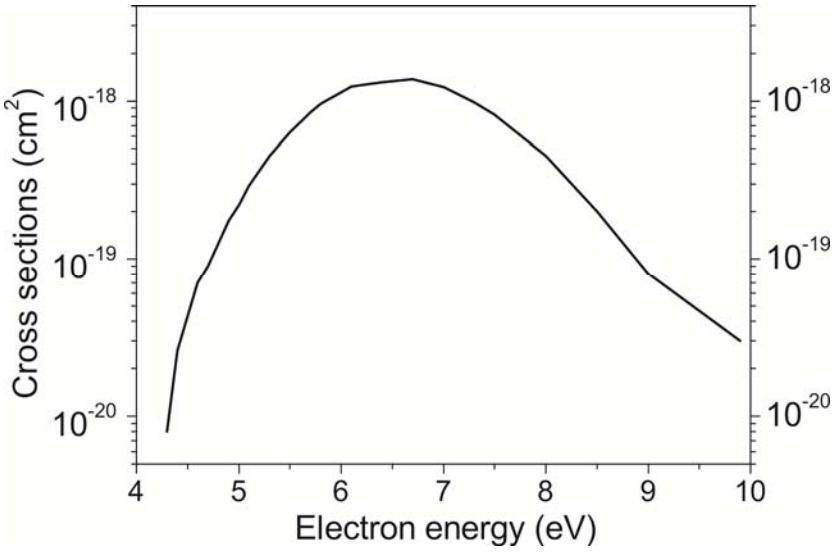

Figure 8-43. Dissociative attachment cross section.

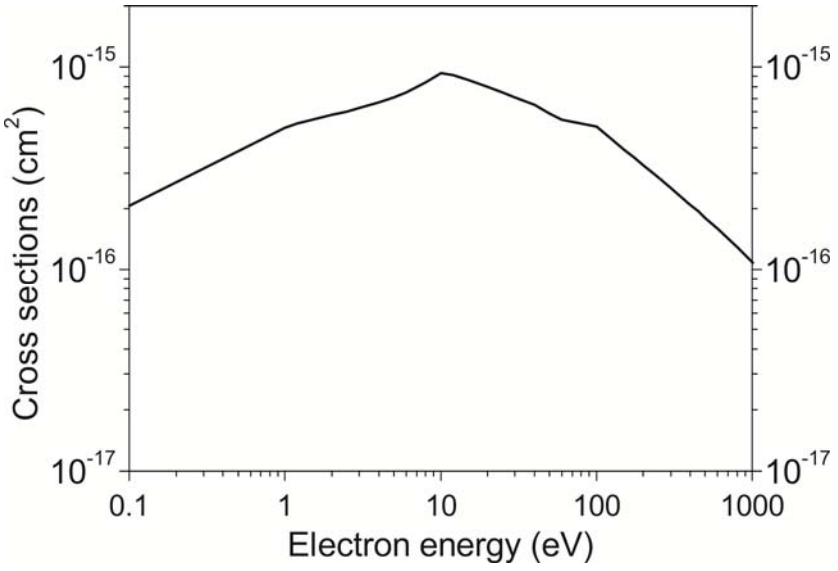

Figure 8-44. Elastic collisions cross sections.